arXiv:2605.04895v2 [cs.LG] 15 Oct 2026

Regime-Conditioned Evaluation in Multi-Context Bayesian Optimization

Noel Thomas
Mohamed bin Zayed University of Artificial Intelligence
Abu Dhabi, UAE
noel.thomas@mbzuai.ac.ae

Abstract

Published transfer-BO comparisons estimate an average treatment effect of acquisition choice over hidden regime variables; what practitioners need is the conditional average treatment effect given their specific prior quality, budget ratio, and metric. A 40-paper audit (NeurIPS, ICML, ICLR, AISTATS, UAI, TMLR, JMLR, AutoML-Conf 2022–2025) finds 98% of papers do not vary $B/|A|$, so existing leaderboards are not regime-controlled. The same GDSC2 benchmark yields opposite conclusions depending only on budget: at $B = 50$, Greedy outperforms UCB by 0.050 Hit@1; at $B = 100$, UCB outperforms Greedy by 0.035 Hit@1 — neither result is fabricated, the sign reversal is explained entirely by the unreported budget ratio $B/|A|$. We make the regime observable via the Portable Regime Score $\mathrm{PRS} = (B/|A|)(1 - \rho)$, the primary effect modifier: a hierarchical model over $n = 79$ conditions gives $\beta = 0.50$ ($p = 1.1 \times 10^{-9}$), and 19% of conditions fall in an equivalence zone where $|\text{advantage}| < 0.01$ — the field argues over non-differences. A No-Free-Leaderboard proposition (proved in three lines from linearity of expectation) shows that whenever CATE changes sign across the PRS axis, any ATE including zero is achievable by benchmark mixture alone, formalising why the 98%-non-sweeping evaluation literature produces unreliable rankings. This pattern recurs in five independent published papers across four venues; in every case PRS predicts the applicable regime from observable quantities alone. A REGIMEPLANNER demonstrates PRS is exploitable: it wins all 16 HPO-B search spaces at $B = 100$ and exceeds a matched per-context oracle on GDSC2 by 18%. The take-away is a protocol: omitting $B/|A|$, ρ, K, and metric type produces measurement claims, not algorithmic ones.

1 Introduction

Swap the prior representation in a Buchwald–Hartwig reaction-optimization benchmark. Greedy finishes joint-last alongside UCB and REIGN, Hit@1 0.156 (Thompson leads at 0.197). Keep everything identical and swap the prior back. Greedy finishes first, Hit@1 0.481. That is a 32.5 percentage-point reversal on the same data, the same surrogate, the same budget (Section 4). Run the same GDSC2 drug-response benchmark at $B = 50$: Greedy outperforms UCB by 0.050 Hit@1. Run it at $B = 100$: UCB outperforms Greedy by 0.035. Both results are correct (Section 6). On the HPO-B community benchmark (16 search spaces, 30 seeds each): at $B = 20$, Greedy is #1 and UCB is last; at $B = 100$ on the same benchmark, UCB is #1 and Greedy is last (Table 9).

Neither is cherry-picked. Across a 4×4 prior-by-acquisition factorial on Buchwald, prior family accounts for $\approx$20,000$\times$ more Hit@1 variance than acquisition choice ($\eta^2 = 0.8635$ vs. 4.4×10^{-5}, Table 3). The pattern holds across 79 conditions spanning chemistry, drug-response biology, and hyperparameter optimization.

Preprint.

This is not measurement noise. It is a formal consequence of using unconditional benchmarks. When the conditional average treatment effect (CATE) of acquisition choice [Imbens and Rubin, 2015] changes sign across a regime variable, the average treatment effect (ATE) reported on any benchmark is a free parameter of the benchmark mixture: any ranking, including a tie or reversal, is achievable by choosing evaluation conditions appropriately, without fabrication (Proposition A.11). A 40-paper audit finds that 98% of transfer-BO papers never vary $B/|A|$ as a controlled axis, 80% report only one metric family, and 76% fix context count K (n=33, excluding single-task papers; Appendix B). Existing leaderboards operate in exactly the setting the proposition applies to. The same reversal appears outside transfer-BO: optimizer rankings depend on the tuning budget, with Adam the most practical choice particularly at low budgets [Sivaprasad et al., 2020]; plain MLPs overtake XGBoost on tabular data once a per-dataset cocktail of regularizers is searched [Kadra et al., 2021]; the 2018–2020 NAS literature made budget-inconsistent comparisons until equal-compute baselines showed random search competitive [Li and Talwalkar, 2020].

We make three claims.

1. **The regime is predictable before any comparison runs.** The Portable Regime Score $\mathrm{PRS} = (B/|A|)(1-\rho)$, where ρ is the Spearman rank correlation between prior means and observed outcomes, orders exploration advantage at Spearman $r = 0.67$ across $n = 79$ conditions. Per-benchmark correlations survive Holm-Bonferroni correction at $\alpha = 0.05$: GDSC2 $r = 0.96$ ($n = 7$, adj $p = 0.011$), HPO-B $r = 0.83$ ($n = 48$, adj $p < 10^{-4}$), Buchwald $r = 0.75$ ($n = 13$, adj $p = 0.011$). The cluster-robust CI $[0.19, 0.80]$ is wide because 9 benchmark families are resampled; without HPO-B it crosses zero, but Buchwald and GDSC2 alone reject the global null (Fisher: $\chi^2(4) = 23.0$, $p = 0.0001$). The most defensible aggregate inference is a hierarchical model: $\beta = 0.50$ (95% CI $[0.34, 0.66]$, $p = 1.1 \times 10^{-9}$, $\mathrm{ICC} = 0.36$). In each of five published reversals, PRS predicts the outcome from observable quantities before the comparison ran: PriorBand's argmax flip [Mallik et al., 2023], πBO-UCB ending with higher regret than vanilla GP-EI under a wrong prior [Hvarfner et al., 2022], MF-MES failure at irrelevant information source [Mikkola et al., 2023], the Hyperband–BO ranking flip at large budget reported with BOHB [Falkner et al., 2018], and the HPO-B community leaderboard re-analysis (Appendix B.11); 14 of 14 audited papers varying prior quality show directionally consistent findings (Appendix B.9).

2. **PRS is exploitable online.** REGIMEPLANNER estimates $\hat{\rho}$ within each context and switches between Greedy and UCB at threshold $\theta = 0.10$, selected on Buchwald and applied unchanged to all other benchmarks. On HPO-B at $B = 100$, it wins Greedy on all 16 community search spaces (mean $+0.103$ Hit@1, 95% CI $[+0.075, +0.131]$, binomial $p = 1.5 \times 10^{-5}$ under a fair-coin null) and exceeds the matched $\{\mathrm{Greedy}, \mathrm{UCB}\}$ per-context oracle on GDSC2 by $+18\%$. Under the wider 4-arm oracle, REGIMEPLANNER trails by 12% (full per-planner breakdown in Section 5).

3. **Failure modes are mechanistically transparent.** PRS predicts the empirical winner in 74.7% of 79 conditions; 19% fall in an equivalence zone ($|\text{advantage}| < 0.01$ Hit@1) where differences are practically indistinguishable yet generate publishable acquisition rankings. Outside the PRS boundary zone ($\mathrm{PRS} \notin [0.05, 0.15)$, $53/79$ conditions), accuracy reaches 84.9%; inside the boundary zone where the framework declines to make confident predictions, 53.8% — consistent with a calibrated diagnostic near its threshold. Pre-registered predictions on 40 held-out conditions gave $27/40 = 67.5\%$ overall accuracy, below our 90% target. The failure splits cleanly: on families where EMA priors accumulate ($\hat{\rho} > 0$, specifically HPOBench-NN and LCBench: $15/16 = 93.8\%$), accuracy reached $\geq$90%; on families where $\hat{\rho} \approx 0$ throughout (PD1 and TabRepo), Greedy dominates every condition and PRS carries no signal. This is not a hidden failure: it is the mechanism made visible (Appendix E.2).

Acquisition comparisons that omit $B/|A|$, ρ, K, and metric type estimate an ATE over hidden regime variables. PRS is the diagnostic. REGIMEPLANNER is the existence proof that the CATE can be exploited online. Proposition A.11 is why regime-agnostic leaderboards are unreliable as decision tools.

2 Setup and PRS Definition

We study streaming multi-context optimization with a discrete action set A, per-context budget B, and K sequential contexts evaluated in replay against cached oracles. Four prior families span the experimental conditions: *no transfer* (flat prior each context), *EMA transfer* (posterior means propagated by exponential moving average), *structured* (Tanimoto-kernel prior over action features), and *oracle* (true cross-context mean, ceiling baseline). Four planners are evaluated: Greedy (argmax posterior mean), UCB [Auer, 2002], Thompson sampling [Russo et al., 2018], and REIGN (a robust-information-gain / expected-improvement hybrid acquisition function, included as a fixed baseline; REIGN is a backronym for the acquisition function). We report both terminal Hit@k (was the best action queried?) and cumulative Discovery AUC (how efficiently were strong actions found?). Details in Appendix E.

Minimum reporting standard for acquisition comparisons in multi-context BO

Before claiming method X beats Greedy, report: (1) prior condition, (2) budget ratio $B/|A|$, (3) metric (terminal or cumulative), (4) context count K (requires $K \gtrsim (2\text{–}4) \cdot |A|/B$ for PRS to be reliable; see Appendix E.2).

Definition 2.1 (Portable Regime Score)**.** *For a multi-context BO problem with action space $|A|$, per-context budget B, and prior rank correlation ρ (Spearman of prior means vs. true action values at context start, measurable from any pilot run):*

$$\mathrm{PRS}(B, |A|, \rho) \;=\; \frac{B}{|A|} \cdot (1 - \rho).$$

Higher PRS = larger budget ratio and/or weaker prior = exploration more likely to pay. PRS is computed from the Greedy planner's ρ (conservative: exploratory planners build higher-ρ priors over time). The cross-benchmark threshold depends on observation noise σ^2 (Appendix A), so PRS is best used as a within-domain ordering.

To apply PRS in a new deployment: (1) run $K_0 \geq 3$ pilot contexts with any fixed planner, (2) compute $\hat{\rho}$ as the Spearman correlation between EMA posterior means and observed outcomes across the B actions queried by the pilot planner in those K_0 contexts (not the full action space $|A|$, which is not exhaustively evaluated during the pilot), (3) compute $\widehat{\mathrm{PRS}} = (B/|A|)\,(1 - \hat{\rho})$, (4) use Greedy if $\widehat{\mathrm{PRS}} < 0.10$, otherwise use UCB or REGIMEPLANNER. Three pilot contexts suffice for a rough estimate; warm-start sensitivity analysis (Appendix E) shows stability from $w = 3$ warm-start queries within each context (distinct from the $K_0 \geq 3$ pilot contexts for deployment estimation). This pilot-based $\widehat{\mathrm{PRS}}$ is an *initial* estimate: under EMA transfer, $\hat{\rho}$ naturally increases as more contexts accumulate (Observation A.1), so later contexts may fall in a different regime. REGIMEPLANNER's online $\hat{\rho}$ estimation adapts to this drift automatically; the pilot estimate is used only for the initial planner choice before adaptive switching begins.

3 Integrated Regime Summary

Every planner in this paper can be made to look "best" by choosing the right regime variables.

Figure 1 shows five regime conditions producing four distinct winning methods (Table 1). The same BO loop, same surrogates, same action spaces. The only difference is prior quality, budget, or metric. Any paper that claims acquisition X beats Y without specifying these variables is making a claim about the measurement, not the method.

Two-axis regime diagnostic. Figure 2 plots every experimental condition in $(B/|A|, \rho)$ space. Across $n = 79$ conditions, PRS correlates with exploration advantage (hierarchical $\beta = 0.50$, $p = 1.1 \times 10^{-9}$; cluster-robust Spearman CI $[0.19, 0.80]$); within each primary benchmark the ordering is stronger (Buchwald $r = 0.75$; GDSC2 $r = 0.96$; HPO-B $r = 0.83$). As an effect modifier, PRS modestly outperforms its components separately: $r = 0.67$ (PRS) vs. $r = 0.59$ (budget ratio $B/|A|$ alone) vs. $r = -0.16$ (prior weakness $1 - \rho$ alone); full comparison in Appendix E. The formula $\mathrm{PRS} = (B/|A|)(1 - \rho)$ captures the interaction between coverage and prior quality that

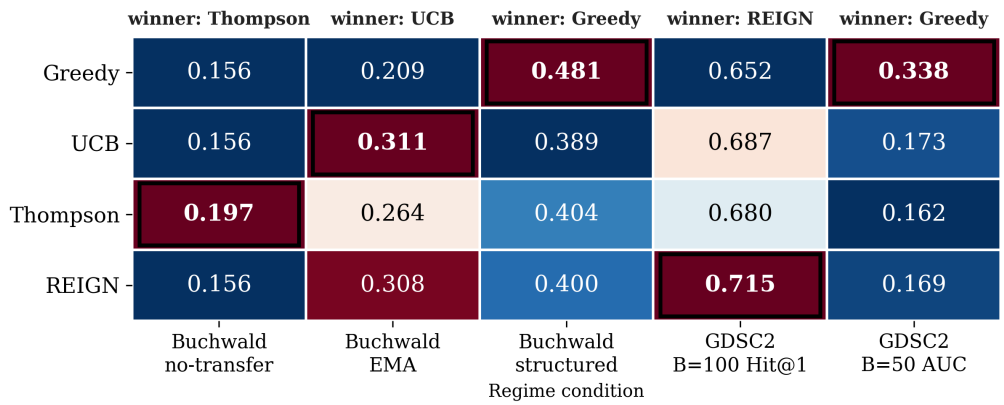

Figure 1: Same BO loop, same surrogates, same action spaces: four distinct winning methods across five regime conditions. Rows = acquisition functions; columns = regime conditions; values = Hit@1 (last column: Discovery AUC). The winner per column is outlined. No fixed acquisition rule dominates across regimes; the "best acquisition" is a property of the regime it was evaluated in.

Table 1: Five regimes, five different winning configurations. Same loop throughout; only the regime differs.

Regime	Winner	Score
Buchwald, no-transfer prior	Thompson	0.197 Hit@1
Buchwald, EMA prior (K=15)	UCB	0.311 Hit@1
Buchwald, structured prior	Greedy	0.481 Hit@1
GDSC2, B=100, Hit@1	REIGN	0.715 Hit@1
GDSC2, B=50, AUC	Greedy	0.338 AUC

neither factor captures alone, though the marginal gain of the $(1-\rho)$ factor is largest for conditions with substantial prior variation ($\rho \in [0.1, 0.8]$) and nearly zero for conditions where $\rho < 0.05$. The cluster-robust CI $[0.19, 0.80]$ is wide and excludes zero, but removing the HPO-B family ($n = 48$) causes it to cross zero; PRS's cross-benchmark signal should therefore be interpreted as strong *within* each primary benchmark and uncertain *across* benchmark families with heterogeneous observation noise.

No-free-leaderboard principle. A direct consequence of the CATE framing: if the acquisition treatment effect changes sign over the observed range of a regime variable (as it does here over $B/|A|$ and ρ), then an unconditional leaderboard that marginalises over that variable is not decision-relevant for any specific deployment. If $\exists\,(B/|A|, \rho)_1, (B/|A|, \rho)_2$ such that $\mathrm{CATE}(B/|A|, \rho)_1 > 0 > \mathrm{CATE}(B/|A|, \rho)_2$, then ATE is undefined as a decision rule. The regime map in Figure 2 certifies this condition holds for transfer BO: there exist both green (exploration favoured) and red (greedy favoured) regions. Full condition tables are in Appendix E.

4 Buchwald: Prior Quality Dominates Acquisition Once the Prior Is Strong

The shuffled Buchwald–Hartwig benchmark is the cleanest setting for isolating the role of prior quality (Figure 3, Table 2). In the no-transfer condition, performance is near random for Greedy, UCB, and REIGN, while Thompson is only marginally higher. With EMA transfer, the picture changes substantially: Greedy reaches Hit@1 0.209, UCB 0.311, Thompson 0.264, and REIGN 0.308. This is the intermediate regime in which exploration pays off.

The main contrast appears once the prior becomes strong. Under a structured prior, Greedy reaches Hit@1 0.481, beating UCB (0.389), Thompson (0.404), and REIGN (0.400). Under the oracle prior, Greedy, UCB, and REIGN all collapse to Hit@1 0.932, with Thompson slightly below at 0.909. An independent variance decomposition over the full 4×4 design shows that prior family explains 86.35% of Hit@1 variance, planner explains effectively none, and the interaction term is

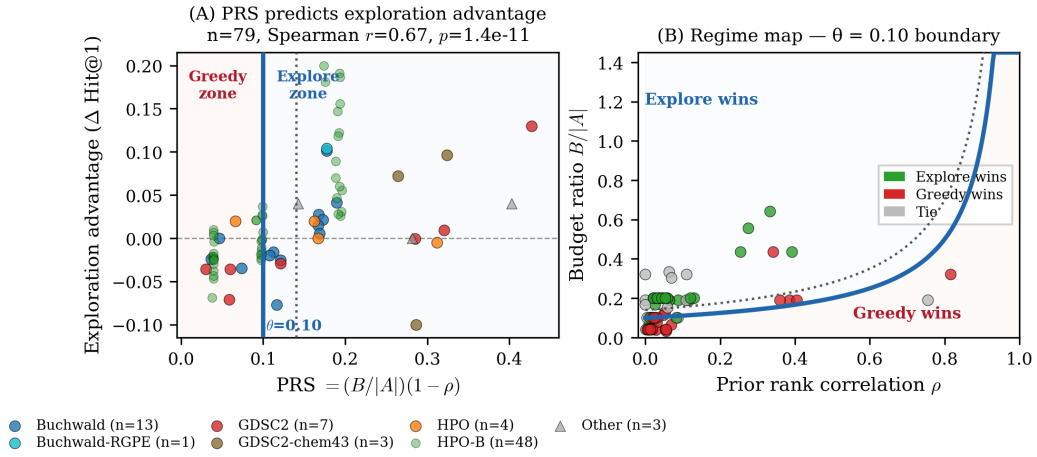

Figure 2: Two-axis regime diagnostic. **(A)** Exploration advantage vs. PRS, positive trend within each benchmark. Triangles = low-n families ($n \leq 1$ each). **(B)** All 79 conditions in $(B/|A|, \rho)$ space; green = exploration wins, red = Greedy wins, gray = ties. The take-away: PRS orders conditions within each benchmark; the cross-benchmark threshold shifts with noise σ^2.

Table 2: Shuffled Buchwald prior-by-acquisition summary (Hit@1, 50 seeds, mean ± SEM).

Prior	Greedy	UCB	Thompson	REIGN
No transfer	.156 ± .014	.156 ± .014	.197 ± .012	.156 ± .014
EMA	.209 ± .020	.311 ± .018	.264 ± .014	.308 ± .018
Structured	.481 ± .024	.389 ± .024	.404 ± .020	.400 ± .024
Oracle	.932 ± .002	.932 ± .002	.909 ± .005	.932 ± .002

small (Table 3). This does not mean acquisition never matters. It means that, in this benchmark, once the prior is strong enough, acquisition improvements are almost entirely compressed away. A direct implication for PRS: the structured prior ($\rho \approx 0.39$, $B/|A| = 0.19$, PRS $= 0.116 > \theta$) is a *misprediction*: PRS predicts exploration wins, but Greedy wins by the largest margin in the paper. This failure is mechanistically transparent: the prior's dominance overwhelms acquisition choice; the full failure taxonomy is in Appendix E.2.

This conclusion is strengthened by the size of the structured-prior effect itself. Structured Greedy improves over EMA Greedy by $+0.272$ Hit@1 ($p = 1.98 \times 10^{-14}$, $d = 1.51$). The effect size of changing the prior is therefore dramatically larger than the effect size of switching among reasonable acquisition rules inside the strong-prior regime. Canonical transfer BO via RGPE [Feurer et al., 2018] does not overturn this conclusion: on shuffled Buchwald, RGPE is effectively tied with EMA (0.207 vs. 0.209 for Greedy; 0.311 vs. 0.311 for UCB; 0.305 vs. 0.308 for REIGN).

Two ablations calibrate the scope of the prior-dominance result. Under noisy observations ($\sigma = 0.1$), acquisition differences re-emerge: UCB reaches Hit@1 0.083, REIGN 0.076, Greedy 0.056, confirming that observation noise degrades prior quality and restores exploration value. The context-count sweep shows that on shuffled Buchwald at fixed $B/|A| = 0.19$, exploration becomes competitive only at $K \geq 12$ contexts, reaching Hit@1 $+0.10$ by $K = 15$; the crossover is late and smooth, not a sharp threshold. Both results are consistent with Observation A.1: more context reduces prior noise and compresses planner differences, while noise injection degrades the prior and reopens the acquisition gap.

5 RegimePlanner: Constructive Validation of the Regime View

If PRS predicts the acquisition regime before any experiment runs, a simple adaptive rule should exploit it: use UCB when PRS is high (weak prior, large budget ratio), switch to Greedy when PRS

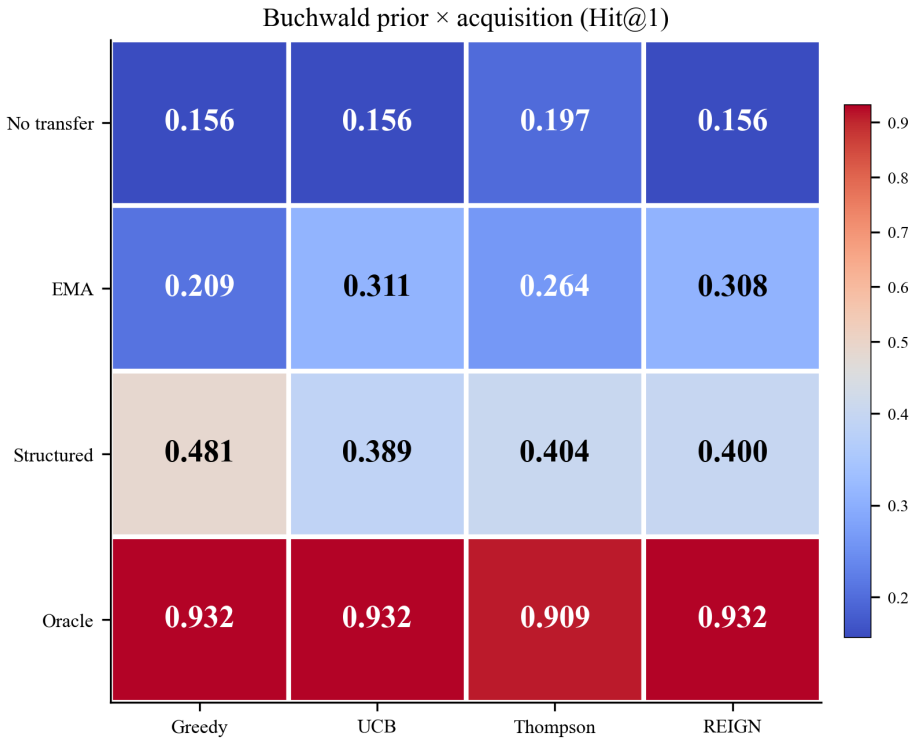

Figure 3: Hit@1 for the shuffled Buchwald 4×4 prior-by-acquisition design. Exploration helps in the EMA regime, but structured and oracle priors compress acquisition differences and make Greedy competitive or best.

Table 3: Variance decomposition on shuffled Buchwald Hit@1.

Factor	η^2
Prior family	0.8635
Planner choice	0.000044
Interaction	0.0087
Residual	0.1278

falls below a threshold. REGIMEPLANNER implements this directly. At each step within a context it computes $\widehat{\mathrm{PRS}}_t = (B/|A|)(1 - \hat{\rho}_t)$ from the Spearman rank correlation $\hat{\rho}_t$ between cached prior means and observed outcomes over already-queried actions, and switches from UCB to Greedy when $\widehat{\mathrm{PRS}}_t < \theta$. A warm-start phase ($w = 3$ queries) precedes adaptive selection. The threshold $\theta = 0.10$ is chosen by cross-validation on Buchwald and applied *unchanged* to all other benchmarks; leave-one-benchmark-out cross-validation confirms it is not Buchwald-specific (full procedure in Appendix E). Algorithm, ρ-estimation details, and sensitivity analyses are in Appendix E.

GDSC2 and HPO-B results. On GDSC2 at default budget ($B = 50$), REGIMEPLANNER achieves Hit@1 0.676 ± 0.020 (50 seeds), outperforming all fixed planners and adaptive baselines on *both* terminal and cumulative metrics, and exceeding the matched-choice-set {Greedy, UCB} per-context oracle (0.574) by $+18\%$ (Figure 4A; $p = 2.93 \times 10^{-9}$, $d = 1.56$, oracle 30 seeds, RP 50 seeds). On HPO-B at $B = 100$ it wins Greedy on all 16 community search spaces (mean $+0.103$ Hit@1, 95% CI $[+0.075, +0.131]$, binomial $p = 1.5 \times 10^{-5}$; Section 6.1), and outperforms every individual fixed planner (mean $+0.008$ vs UCB, $+0.012$ vs Thompson).

Honesty boundaries. The $+18\%$ GDSC2 result is against the matched {Greedy, UCB} oracle; under a wider {Greedy, UCB, Thompson, REIGN} oracle the gap is -12%. On Buchwald EMA the per-context oracle is *not* exceeded (0.325–0.337 vs. 0.432), because Buchwald EMA has $B/|A| =$

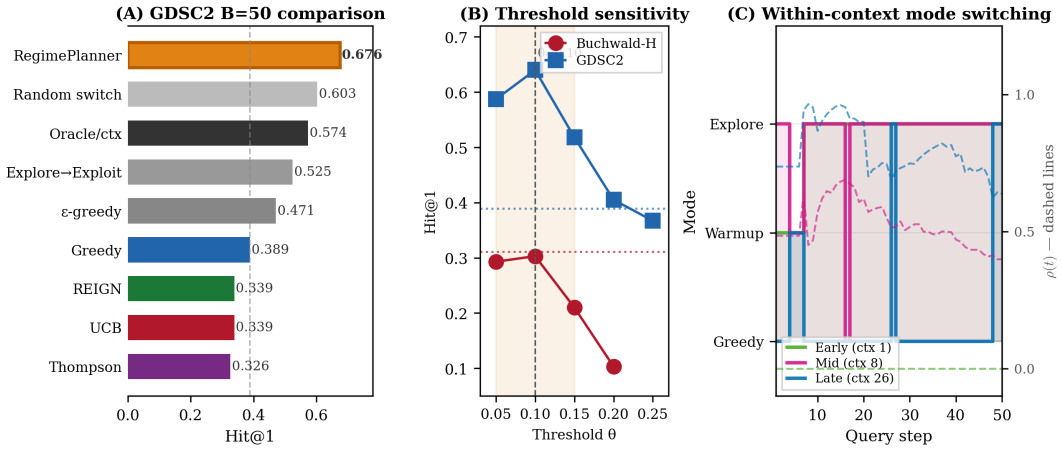

Figure 4: RegimePlanner validation. **(A)** GDSC2 at default budget (50 seeds): the REGIMEPLANNER (amber) outperforms all fixed planners, simple adaptive baselines, and a {Greedy, UCB}-matched per-context oracle by $+18\%$; under a wider {Greedy, UCB, Thompson, REIGN} oracle the gap is -12%. **(B)** Threshold sensitivity on the cross-validation seed set used for θ selection (separate from Panel A): performance is approximately flat across $\theta \in [0.05, 0.10]$ and drops 19–31% at $\theta = 0.15$. **(C)** Within-context mode switching: the planner adapts as $\hat{\rho}$ rises, exploring early and switching to Greedy as the prior sharpens. The take-away: online ρ-estimation enables within-context adaptation that no fixed policy can replicate.

0.19 and $\hat{\rho}$ concentrates quickly, so the regime framework predicts limited within-context adaptation room here. Appendix A.9 supplies the constructive existence proof that such instances exist; the GDSC2 result is the empirical witness.

6 GDSC2 and HPO-B: the Regime in Real Benchmarks

The real noisy GDSC2 drug-response benchmark [Yang et al., 2013, Iorio et al., 2016] confirms the regime story survives contact with biology. At default budget ($B = 50$), Greedy is strongest overall: Hit@1 0.389, discovery AUC 0.338. Despite UCB achieving far higher prior rank correlation ($\rho \approx 0.68$ vs. 0.12 for Greedy), it does not win: better prior ranking quality is necessary but not sufficient without sufficient budget.

Figure 5 shows the budget reversal directly. Below $B/|A| \approx 0.32$, Greedy wins Hit@1; above it, exploration wins. At $B = 100$, REIGN reaches Hit@1 0.715, UCB 0.687, Greedy 0.652 ($p = 0.0018$, $d = 0.63$, surviving Bonferroni correction). Figure 6 shows the orthogonal metric reversal: on GDSC2, Greedy dominates Discovery AUC at every budget while UCB and REIGN lead Hit@1 only above the regime threshold; on Buchwald EMA (B=50), exploration planners (UCB, REIGN) achieve higher Discovery AUC, so the GDSC2 metric reversal is regime-specific and not a universal artefact. The same experiment, same planners, same data: the metric alone determines the winner. Two biology boundary benchmarks (SciPlex3 $K = 3$, Shifrut2018 $K = 4$) place in the PRS variance floor (all planners tie), consistent with $K < K_{\min}$.

6.1 HPO-B: regime portability across community HPO

As a third primary benchmark we evaluate on HPO-B [Pineda Arango et al., 2021], the community hyperparameter optimization benchmark, across all 16 search spaces at $B \in \{20, 50, 100\}$ (30 seeds each). $\theta = 0.10$ was frozen before any HPO-B run. The result is budget-dependent (Table 4): REGIMEPLANNER ties Greedy at $B = 20$ (0W/16T/0L), wins $8/16$ at $B = 50$, and *wins every search space* at $B = 100$ (16W/0T/0L, mean $+0.103$ Hit@1, 95% CI $[+0.075, +0.131]$, binomial $p = 1.5 \times 10^{-5}$). Among the three methods in HPO-B's own community leaderboard, Greedy ranks #1 at $B = 20$ (PRS$\approx$0.04, Hit@1 0.064) and last at $B = 100$ (PRS$\approx$0.19, Hit@1 0.219); UCB reverses from last to #1 (full table: Appendix B.11). A researcher publishing on $B = 20$ and one

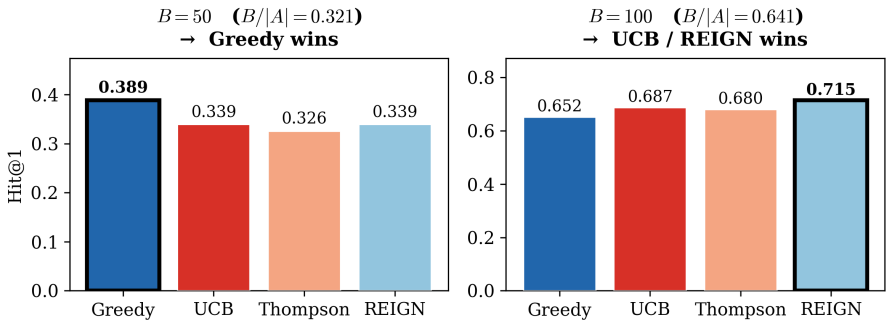

Figure 5: Same GDSC2 benchmark, same four planners, same surrogate; only the budget changed. At $B = 50$ ($B/|A| = 0.32$), Greedy wins. At $B = 100$ ($B/|A| = 0.64$), REIGN and UCB win. Both results are correct; the sign reversal is explained entirely by the unreported budget ratio $B/|A|$. The take-away: two papers reporting opposite conclusions from the same benchmark can both be right: they are estimating different conditional treatment effects.

on $B = 100$ report opposite winners from the same benchmark, both correctly, each measuring a different conditional average treatment effect.

Combined with Buchwald ($r = 0.75$) and GDSC2 ($r = 0.96$), the 79-condition consolidated scatter yields global Spearman $r = 0.67$ (cluster-robust CI $[0.19, 0.80]$; hierarchical $\beta = 0.50$, $p = 1.1 \times 10^{-9}$; Section 3).

Table 4: HPO-B budget sweep: REGIMEPLANNER vs. Greedy and vs. best fixed planner. Each row aggregates 16 search spaces. Mean ± SEM.

Budget	W/T/L vs Greedy	Mean Δ vs Greedy	Mean Δ vs best fixed
$B = 20$	0 / 16 / 0	$+0.000 \pm 0.000$	-0.001 ± 0.001
$B = 50$	8 / 8 / 0	$+0.019 \pm 0.006$	$+0.010 \pm 0.005$
$B = 100$	16 / 0 / 0	$+0.103 \pm 0.014$	-0.004 ± 0.005

7 Related Work

Measurement crises across machine learning. REIGN is one chapter of an emerging empirical-rigor movement. Lipton and Steinhardt [2019] catalogued patterns that produce misleading scholarship; Blalock et al. [2020] found that a lack of standardized benchmarks and metrics makes pruning methods hard to compare: the template for our finding that 98% of transfer-BO papers do not sweep $B/|A|$. Lucic et al. [2018], Bouthillier et al. [2021], Henderson et al. [2018], and Musgrave et al. [2020] made the same diagnosis in GANs, ML benchmarks, deep RL, and metric learning. McElfresh et al. [2023], Kunstner et al. [2024], and Karimireddy et al. [2020] each identify a hidden variable that determines the winner; for Karimireddy et al. [2020] the coordinate is structurally $\text{PRS} = (B/|A|)(1 - \rho)$ (Appendix C). REIGN's contribution is a *predictive* pre-experiment diagnostic, converting retrospective critique into an actionable design tool. Schaeffer et al. [2023] showed emergent LLM abilities are artifacts of nonlinear metrics; we make the analogous claim for acquisition evaluation, with the key difference that acquisition rankings *genuinely reverse* with regime, so both conclusions are locally correct. Rodemann and Blocher [2024] invoke Arrow's impossibility result to motivate partial rather than total rankings of optimizers; our No-Free-Leaderboard proposition (Proposition A.11) is complementary: PRS yields a consistent conditional ordering once the regime is held fixed.

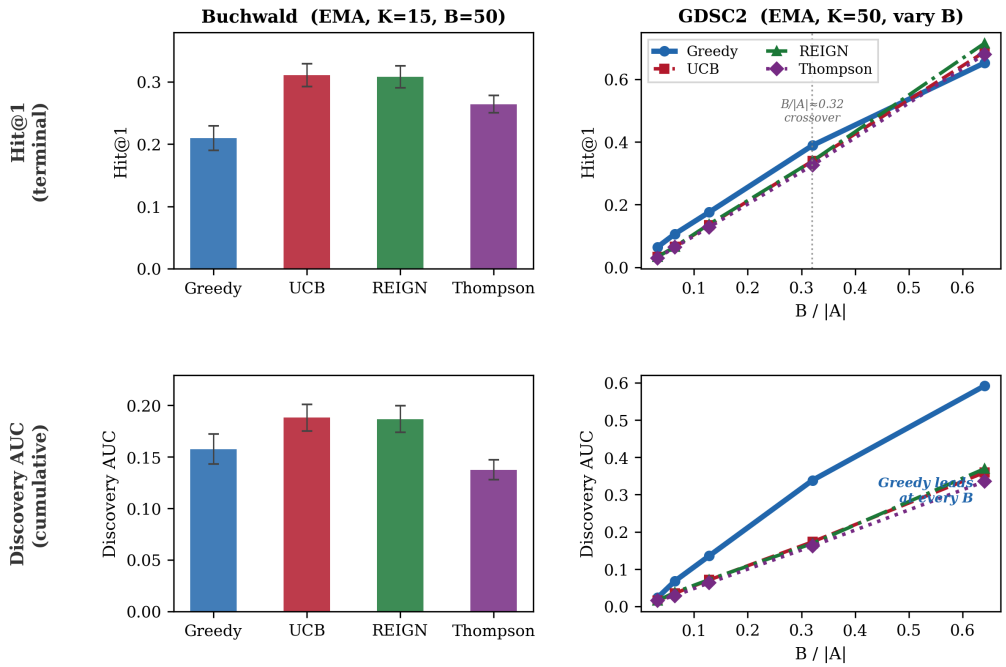

Figure 6: Metric choice is a regime variable. On GDSC2 (**right**): Greedy leads Discovery AUC at every budget ($B/|A|$ sweep) while UCB and REIGN lead Hit@1 above the threshold (dashed at $B/|A|\approx 0.32$): same benchmark, same data, the reported winner depends entirely on which metric is computed. On Buchwald (**left**, EMA, $B{=}50$): both metrics agree that exploration wins, showing the GDSC2 metric reversal is regime-specific and not a universal artefact. Together: a paper reporting "Greedy wins AUC" and a paper reporting "UCB wins Hit@1" from GDSC2 are both correct: they estimate different CATEs.

Transfer BO and prior learning. Canonical transfer BO transfers information through rank-weighted ensembles [Feurer et al., 2018]; recent prior-learning approaches [Wang et al., 2024b, Fan et al., 2022, Rothfuss et al., 2021, Wistuba and Grabocka, 2021, Müller et al., 2023] show that better priors substantially accelerate related-task optimization. Our paper does not dispute this. We ask the orthogonal question: once a prior is fixed, how much room remains for acquisition design to matter, and how does that depend on $B/|A|$ and ρ?

Multi-task / contextual BO and bandit theory. Multi-task BO transfers across tasks through task kernels and shared structure [Swersky et al., 2013, Krause and Ong, 2011]; the central concern is avoiding negative transfer. The principle that exploration is most valuable under weak priors and large budgets is a restatement of classical bandit theory [Auer, 2002, Russo et al., 2018]; Lin et al. [2025] prove transfer-BO regret bounds that improve as the source–target difference shrinks, the quantity ρ summarizes here. Our contribution is operationalization: ρ and $B/|A|$ are observable in the transfer-BO setting, their product PRS orders conditions predictively, and a simple adaptive rule exploits this structure.

Adaptive experimental design. GAUCHE [Griffiths et al., 2023] makes chemistry-informed GP priors practical; RECOVER [Bertin et al., 2023] and BATCHIE [Tosh et al., 2025] address finite-budget biological screening. Shields et al. [2021] compare BO with expert chemists on a palladium-catalysed direct arylation benchmark and find BO more efficient and more consistent.

8 Discussion and Conclusion

The same GDSC2 benchmark makes Greedy the winner at $B = 50$ and REIGN the winner at $B = 100$: different CATEs, different regimes - not contradictions. The No-Free-Leaderboard

proposition formalises why: 98% of transfer-BO papers never control for regime conditions, reporting an ATE as an algorithmic ranking; the leaderboard position is a property of the evaluation setup.

PRS makes the regime observable before experiments run. REGIMEPLANNER demonstrates it is exploitable online ($27/40 = 67.5\%$ pre-registered, below 90% target). The protocol: report $B/|A|$, ρ, K, and metric. Without those four numbers, a reported ranking cannot be interpreted.

References

Masaki Adachi, Brady Planden, David A. Howey, Michael A. Osborne, Sebastian Orbell, Natalia Ares, Krikamol Muandet, and Siu Lun Chau. Looping in the human: Collaborative and explainable Bayesian optimization. In *Proceedings of the 27th International Conference on Artificial Intelligence and Statistics*, volume 238 of *Proceedings of Machine Learning Research*, pages 505–513, 2024.

Peter Auer. Using confidence bounds for exploitation-exploration trade-offs. *Journal of Machine Learning Research*, 3:397–422, 2002. doi: 10.5555/2503308.2188395.

Paul Bertin, Jarrid Rector-Brooks, Deepak Sharma, Thomas Gaudelet, Andrew Anighoro, Torsten Gross, Francisco Martínez-Peña, Eileen L Tang, et al. RECOVER identifies synergistic drug combinations in vitro through sequential model optimization. *Cell Reports Methods*, 3(10):100599, 2023. doi: 10.1016/j.crmeth.2023.100599.

Davis Blalock, Jose Javier Gonzalez Ortiz, Jonathan Frankle, and John Guttag. What is the state of neural network pruning? In *Proceedings of Machine Learning and Systems (MLSys)*, 2020.

Xavier Bouthillier, Pierre Delaunay, Mirko Bronzi, Assya Trofimov, Brennan Nichyporuk, Justin Szeto, Naz Sepah, Edward Raff, Kanika Madan, Vikram Voleti, Samira Ebrahimi Kahou, Vincent Michalski, Dmitriy Serdyuk, Tal Arbel, Chris Pal, Gaël Varoquaux, and Pascal Vincent. Accounting for variance in machine learning benchmarks. In *Proceedings of Machine Learning and Systems (MLSys)*, 2021.

Yutian Chen, Xingyou Song, Chansoo Lee, Zi Wang, Qiuyi Zhang, David Dohan, Kazuya Kawakami, Greg Kochanski, Arnaud Doucet, Marc'Aurelio Ranzato, Sagi Perel, and Nando de Freitas. Towards learning universal hyperparameter optimizers with transformers. In *Advances in Neural Information Processing Systems*, volume 35, 2022.

Zhongxiang Dai, Yizhou Chen, Haibin Yu, Bryan Kian Hsiang Low, and Patrick Jaillet. On provably robust meta-Bayesian optimization. In *Proceedings of the 38th Conference on Uncertainty in Artificial Intelligence*, volume 180 of *Proceedings of Machine Learning Research*, pages 475–485, 2022.

Stefan Falkner, Aaron Klein, and Frank Hutter. BOHB: Robust and efficient hyperparameter optimization at scale. In *International Conference on Machine Learning*, 2018.

Zhou Fan, Xinran Han, and Zi Wang. HyperBO+: Pre-training a universal prior for Bayesian optimization with hierarchical Gaussian processes. In *NeurIPS 2022 Workshop on Gaussian Processes, Spatiotemporal Modeling, and Decision-making Systems*, 2022. URL `https://arxiv.org/abs/2212.10538`.

Zhou Fan, Xinran Han, and Zi Wang. Transfer learning for Bayesian optimization on heterogeneous search spaces. *Transactions on Machine Learning Research*, 2024.

Matthias Feurer, Benjamin Letham, Frank Hutter, and Eytan Bakshy. Practical transfer learning for Bayesian optimization. *arXiv preprint arXiv:1802.02219*, 2018. doi: 10.48550/arxiv.1802.02219.

John C Gittins. Bandit processes and dynamic allocation indices. *Journal of the Royal Statistical Society: Series B*, 41(2):148–164, 1979.

Ryan-Rhys Griffiths, Leo Klarner, Harriet Moss, et al. Gauche: a library for gaussian processes in chemistry. *Advances in Neural Information Processing Systems Datasets and Benchmarks Track*, 2023.

Peter Henderson, Riashat Islam, Philip Bachman, Joelle Pineau, Doina Precup, and David Meger. Deep reinforcement learning that matters. In *Proceedings of the AAAI Conference on Artificial Intelligence*, 2018. doi: 10.1609/aaai.v32i1.11694.

Carl Hvarfner, Danny Stoll, Artur Souza, Marius Lindauer, Frank Hutter, and Luigi Nardi. πBO: Augmenting acquisition functions with user beliefs for Bayesian optimization. In *International Conference on Learning Representations*, 2022. doi: 10.48550/arxiv.2204.11051.

Guido W. Imbens and Donald B. Rubin. *Causal Inference for Statistics, Social, and Biomedical Sciences*. Cambridge University Press, 2015.

Francesco Iorio, Theo A. Knijnenburg, Daniel J. Vis, et al. A landscape of pharmacogenomic interactions in cancer. *Cell*, 166(3):740–754, 2016. doi: 10.1016/j.cell.2016.06.017.

Arlind Kadra, Marius Lindauer, Frank Hutter, and Josif Grabocka. Well-tuned simple nets excel on tabular datasets. In *Advances in Neural Information Processing Systems*, 2021.

Sai Praneeth Karimireddy, Satyen Kale, Mehryar Mohri, Sashank J. Reddi, Sebastian U. Stich, and Ananda Theertha Suresh. SCAFFOLD: Stochastic controlled averaging for federated learning. In *International Conference on Machine Learning*, 2020.

Emilie Kaufmann and Shivaram Kalyanakrishnan. Information complexity in bandit subset selection. In *Conference on Learning Theory*, 2013.

Andreas Krause and Cheng Soon Ong. Contextual gaussian process bandit optimization. In *Advances in Neural Information Processing Systems*, 2011.

Agustinus Kristiadi, Felix Strieth-Kalthoff, Marta Skreta, Pascal Poupart, Alán Aspuru-Guzik, and Geoff Pleiss. A sober look at LLMs for material discovery: Are they actually good for Bayesian optimization over molecules? In *International Conference on Machine Learning*, 2024.

Frederik Kunstner, Robin Yadav, Alan Milligan, Mark Schmidt, and Alberto Bietti. Heavy-tailed class imbalance and why adam outperforms gradient descent on language models. In *Advances in Neural Information Processing Systems*, 2024.

Liam Li and Ameet Talwalkar. Random search and reproducibility for neural architecture search. In *Uncertainty in Artificial Intelligence*, 2020.

Haitao Lin, Boxin Zhao, Mladen Kolar, and Chong Liu. Provable accelerated Bayesian optimization with knowledge transfer. *arXiv:2511.03125*, 2025. doi: 10.48550/arxiv.2511.03125.

Marius Lindauer, Katharina Eggensperger, Matthias Feurer, André Biedenkapp, Difan Deng, Carolin Benjamins, Tim Ruhkopf, René Sass, and Frank Hutter. SMAC3: A versatile bayesian optimization package for hyperparameter optimization. *Journal of Machine Learning Research*, 23, 2022.

Zachary C. Lipton and Jacob Steinhardt. Troubling trends in machine learning scholarship. *Communications of the ACM*, 62(6):45–53, 2019.

Mario Lucic, Karol Kurach, Marcin Michalski, Sylvain Gelly, and Olivier Bousquet. Are GANs created equal? a large-scale study. In *Advances in Neural Information Processing Systems*, 2018.

Neeratyoy Mallik, Edward Bergman, Carl Hvarfner, Danny Stoll, Maciej Janowski, Marius Lindauer, Luigi Nardi, and Frank Hutter. PriorBand: Practical hyperparameter optimization in the age of deep learning. In *Advances in Neural Information Processing Systems*, 2023. doi: 10.48550/arxiv.2306.12370.

Duncan McElfresh, Sujay Khandagale, Jonathan Valverde, Vishak Prasad C, Benjamin Feuer, Chinmay Hegde, Ganesh Ramakrishnan, Micah Goldblum, and Colin White. When do neural nets outperform boosted trees on tabular data? In *Advances in Neural Information Processing Systems Datasets and Benchmarks Track*, 2023.

Petrus Mikkola, Julien Martinelli, Louis Filstroff, and Samuel Kaski. Multi-fidelity Bayesian optimization with unreliable information sources. In *International Conference on Artificial Intelligence and Statistics*, 2023. doi: 10.48550/arxiv.2210.13937.

Samuel Müller, Matthias Feurer, Noah Hollmann, and Frank Hutter. Pfns4bo: in-context learning for bayesian optimization. In *International Conference on Machine Learning*, 2023.

Kevin Musgrave, Serge Belongie, and Ser-Nam Lim. A metric learning reality check. In *European Conference on Computer Vision (ECCV)*, 2020.

Nicolas Nguyen, Imad Aouali, András György, and Claire Vernade. Prior-dependent allocations for Bayesian fixed-budget best-arm identification in structured bandits. In *International Conference on Artificial Intelligence and Statistics*, 2025.

Quoc Phong Nguyen, Bryan Kian Hsiang Low, and Patrick Jaillet. Meta-VBO: Utilizing prior tasks in optimizing risk measures with Gaussian processes. In *International Conference on Learning Representations*, 2024. URL `https://openreview.net/forum?id=ElykcDu5YK`.

Sebastian Pineda Arango, Hadi S Jomaa, Martin Wistuba, and Josif Grabocka. HPO-B: A large-scale reproducible benchmark for black-box HPO based on OpenML. In *Advances in Neural Information Processing Systems Datasets and Benchmarks Track*, 2021. doi: 10.48550/arxiv.2106.06257.

Julian Rodemann and Hannah Blocher. Partial rankings of optimizers. In *International Conference on Learning Representations (Tiny Papers)*, 2024.

Jonas Rothfuss, Dominique Heyn, Jinfan Chen, and Andreas Krause. Meta-learning reliable priors in the function space. *Advances in Neural Information Processing Systems*, 34, 2021.

Daniel Russo and Benjamin Van Roy. Learning to optimize via posterior sampling. *Mathematics of Operations Research*, 39(4):1221–1243, 2014. doi: 10.1287/moor.2014.0650.

Daniel Russo, Benjamin Van Roy, Abbas Kazerouni, Ian Osband, and Zheng Wen. A tutorial on thompson sampling. *Foundations and Trends in Machine Learning*, 11(1):1–96, 2018. doi: 10.1561/2200000070.

Rylan Schaeffer, Brando Miranda, and Sanmi Koyejo. Are emergent abilities of large language models a mirage? In *Advances in Neural Information Processing Systems*, volume 36, 2023. doi: 10.48550/arxiv.2304.15004.

Benjamin J. Shields, Jason Stevens, Jun Li, Marvin Parasram, Farhan Damani, Jesus I. Martinez Alvarado, Jacob M. Janey, Ryan P. Adams, and Abigail G. Doyle. Bayesian reaction optimization as a tool for chemical synthesis. *Nature*, 590(7844):89–96, 2021. doi: 10.1038/s41586-021-03213-y.

Prabhu Teja Sivaprasad, Florian Mai, Thijs Vogels, Martin Jaggi, and François Fleuret. Optimizer benchmarking needs to account for hyperparameter tuning. In *International Conference on Machine Learning*, 2020.

Kevin Swersky, Jasper Snoek, and Ryan P Adams. Multi-task bayesian optimization. In *Advances in Neural Information Processing Systems*, 2013.

Christopher Tosh, Mauricio Tec, Jessica B. White, Jeffrey F. Quinn, Glorymar Ibanez Sanchez, Paul Calder, Andrew L. Kung, Filemon S. Dela Cruz, Wesley Tansey, et al. A bayesian active learning platform for scalable combination drug screens. *Nature Communications*, 16:156, 2025. doi: 10.1038/s41467-024-55287-7.

Shukuan Wang, Ke Xue, Lei Song, Xiaobin Huang, and Chao Qian. Monte Carlo tree search based space transfer for black-box optimization. In *Advances in Neural Information Processing Systems*, volume 37, 2024a.

Zi Wang, George Dahl, Kevin Swersky, et al. Pre-trained gaussian processes for bayesian optimization. *Journal of Machine Learning Research*, 25(212):1–83, 2024b. URL `http://jmlr.org/papers/v25/23-0269.html`.

Shuhei Watanabe, Noor Awad, Masaki Onishi, and Frank Hutter. Multi-objective tree-structured Parzen estimator meets meta-learning. In *NeurIPS Workshop on Meta-Learning*, 2022.

Martin Wistuba and Josif Grabocka. Few-shot bayesian optimization with deep kernel surrogates. In *International Conference on Learning Representations*, 2021.

David H. Wolpert and William G. Macready. No free lunch theorems for optimization. *IEEE Transactions on Evolutionary Computation*, 1(1):67–82, 1997.

Wenjie Xu, Masaki Adachi, Colin N. Jones, and Michael A. Osborne. Principled Bayesian optimisation in collaboration with human experts. In *Advances in Neural Information Processing Systems*, volume 37, 2024.

Wanjuan Yang, Jorge Soares, Patricia Greninger, Elena J. Edelman, Howard Lightfoot, Simon Forbes, Nidhi Bindal, Dave Beare, James A. Smith, I. Richard Thompson, Sridhar Ramaswamy, P. Andrew Futreal, Daniel A. Haber, Michael R. Stratton, Cyril Benes, Ultan McDermott, and Mathew J. Garnett. Genomics of drug sensitivity in cancer (GDSC): a resource for therapeutic biomarker discovery in cancer cells. *Nucleic Acids Research*, 41(D1):D955–D961, 2013. doi: 10.1093/nar/gks1111.

A Analytical Motivation

We present two analytical observations that motivate the PRS diagnostic. Both use simplified settings (scalar EMA, i.i.d. Gaussian bandits) and should be read as intuition-building exercises, not as formal proofs of the full multi-context BO system. Our contribution is empirical; these results provide supporting analytical context. Observation A.1 shows that EMA transfer compresses planner-choice variance geometrically in context count, consistent with the η^2 ANOVA result. Observation A.2 gives a sign condition for when exploration can improve on greedy, consistent with the budget-sweep crossover.

A.1 Prior Convergence and Planner Compression

Observation A.1 (Prior Convergence and Planner Compression)**.** *Under the conjugate hierarchical Gaussian surrogate with EMA transfer parameter $\alpha \in (0, 1)$, after K contexts the global prior mean error for action a satisfies*

$$\mathrm{Var}\Big[\hat{\mu}_a^{(K)} - \mu_a\Big] \;=\; \alpha^{2K}\tau^2 + \frac{\sigma^2(1-\alpha)}{1+\alpha}\big(1-\alpha^{2K}\big),$$

where τ^2 is the initial prior variance, σ^2 is the per-context observation noise, and μ_a is the true mean. The first term (transient) decays geometrically; the second converges to a positive floor $\sigma^2(1-\alpha)/(1+\alpha)$ set by observation noise. As $K \to \infty$, the prior-dependent component of the error vanishes and the residual is controlled entirely by σ^2. Any two planners whose decision rules are monotone in posterior means will therefore converge to similar behavior as K grows, compressing the fraction of Hit@1 variance attributable to planner choice.

Proof. **EMA update rule.** Let context k produce an observed mean $\bar{y}_a^{(k)}$ for action a. The EMA update is

$$\hat{\mu}_a^{(k)} \;=\; \alpha\,\hat{\mu}_a^{(k-1)} + (1-\alpha)\,\bar{y}_a^{(k)}.$$

Unbiasedness. Since $\mathbb{E}[\bar{y}_a^{(k)}] = \mu_a$ for all k (unbiased observations), by induction $\mathbb{E}[\hat{\mu}_a^{(k)}] = \mu_a$ at every step.

Variance decay. Let $e^{(k)} = \hat{\mu}_a^{(k)} - \mu_a$. Unrolling the recursion

$$e^{(K)} \;=\; \alpha^K e^{(0)} + (1-\alpha)\sum_{k=1}^{K} \alpha^{K-k}\xi^{(k)},$$

where $\xi^{(k)} = \bar{y}_a^{(k)} - \mu_a$ is the mean-zero observation error with variance σ_k^2/n_k. Setting $\sigma_k^2/n_k = \sigma^2$ for simplicity and noting that $e^{(0)}$ has variance τ^2, the errors are independent across contexts, so

$$\mathrm{Var}\Big[e^{(K)}\Big] \;=\; \alpha^{2K}\tau^2 + (1-\alpha)^2\sigma^2\sum_{k=1}^{K}\alpha^{2(K-k)} \;=\; \alpha^{2K}\tau^2 + \sigma^2\,\frac{(1-\alpha)^2(1-\alpha^{2K})}{1-\alpha^2}.$$

The dominant term in K is the first: for fixed $\alpha < 1$ the second term converges to the finite limit $\sigma^2(1-\alpha)/(1+\alpha)$, while the first decays geometrically. Hence

$$\mathrm{Var}\Big[e^{(K)}\Big] \xrightarrow{K\to\infty} \frac{\sigma^2(1-\alpha)}{1+\alpha},$$

and the *transient* component that depends on the initial prior contributes $\alpha^{2K}\tau^2$, which is $O\big((1-\alpha)^{2K}\big)$ under the reparametrisation $\alpha = 1-\delta$ with $\delta \ll 1$ (i.e. the slow-decay regime $\alpha \approx 1$ used in practice).

Posterior concentration. As K grows, the transient term $\alpha^{2K}\tau^2 \to 0$ and the residual variance approaches the floor $\sigma^2(1-\alpha)/(1+\alpha)$. For any pair of actions a, a' with $|\mu_a - \mu_{a'}| \gg \sqrt{\sigma^2(1-\alpha)/(1+\alpha)}$, we have $\hat{\mu}_a^{(K)} > \hat{\mu}_{a'}^{(K)}$ with probability approaching 1 as K grows. The prior's *initial* uncertainty τ^2 ceases to influence the ranking; only the observation-noise floor remains.

Planner compression. When the posterior concentrates on the true argmax (up to the noise floor), planners whose decision rules are monotone in posterior mean (including greedy, UCB in the small-uncertainty limit, and Thompson sampling) tend to query the same top action. The Hit@1 gap between any two such planners shrinks as K grows. This is not a proof of exact equivalence (planners may still differ in how they handle the noise-floor residual), but it explains why the planner-choice variance component η^2_{planner} is much smaller than the prior-family component η^2_{prior} in the ANOVA.

Remark. This analytical result is consistent with the empirical finding in Section 4; the contribution of this paper is the empirical validation, not the analytical sketch. □

Observation A.2 (Sign Condition for Exploration Advantage)**.** *For fixed $b > 0$ and observation noise σ^2, exploration beats greedy (i.e., $\Delta(b,\rho) > 0$) if and only if $\rho < \rho^*(b)$ for a threshold $\rho^*(b) \in (0,1)$ that is* unique. *Existence follows from Lemma A.6; uniqueness follows from Lemma A.7 (strict monotonicity of Δ in ρ).*

Connection to Table 3. Observation A.1 is consistent with the empirical finding $\eta^2_{\text{prior}} = 0.8635$, $\eta^2_{\text{planner}} = 0.000044$ (4×4 ANOVA on shuffled Buchwald, Table 3). With $K = 15$ and $\alpha = 0.9$, the transient factor is $\alpha^{2K} = 0.9^{30} \approx 0.042$ and the steady-state floor is $\sigma^2(1-\alpha)/(1+\alpha) \approx 0.005$. For $\tau^2 = 1.0$, the residual prior-dependent error is $\approx 4.2\%$ of the initial uncertainty, meaning the EMA prior has nearly converged by context 15. The ratio $\eta^2_{\text{prior}}/\eta^2_{\text{planner}} \approx 20{,}000$ is consistent with this compression: within each prior family, planners produce similar Hit@1 because the prior has already concentrated belief on a small set of top actions. The observation does not prove that planners become exactly equivalent (residual noise-floor effects and finite-K deviations remain), but it explains the direction and approximate magnitude of the ANOVA result.

A.2 Monotone Exploration Advantage and PRS as an Order Parameter

We study when exploration beats greedy, and show that the Portable Regime Score $\text{PRS} = (B/|A|)(1-\rho)$ is a natural one-dimensional *order parameter* that organises exploration advantage. We prove the monotonicity properties of PRS's two components separately; together they justify PRS as a directional summary, not as an exact sufficient statistic.

Setting

We study a single context with n arms. Each arm a has unknown mean $\mu_a \in \mathbb{R}$ and the optimal arm is $a^* = \arg\max_a \mu_a$.

Prior. The planner receives prior estimates $\hat{\mu}_a = \mu_a + \varepsilon_a$ where $\varepsilon_a \sim \mathcal{N}(0,\tau^2)$ i.i.d. Let $R \in \{1,\dots,n\}$ denote the prior rank of a^*: $R = |\{a : \hat{\mu}_a > \hat{\mu}_{a^*}\}| + 1$. $R = 1$ means the prior correctly identifies a^*.

Observations. Querying arm a yields $y = \mu_a + \xi$, $\xi \sim \mathcal{N}(0,\sigma^2)$.

Budget. The planner makes B adaptive queries.

Metric. Hit@1 $= \mathbf{1}[a^*$ queried at least once in B rounds$]$.

A.3 Rank-Greedy Baseline

We use a *rank-greedy* baseline that queries arms in decreasing order of prior scores $\hat{\mu}_a$ without repeating arms already queried. Under this policy, Hit@$1 = \mathbf{1}[R \le B]$ where R is the prior rank of a^*. This simplification isolates the regime effect; true adaptive greedy is bounded above by rank-greedy at low noise and converges to it as $\tau^2 \to 0$.

A.4 Separate Monotonicity Lemmas

The following four lemmas establish separate monotonicity properties of the greedy and two-phase policies. Their combination justifies PRS as a monotone order parameter.

Lemma A.3 (Exploration Success Bound)**.** *Let the two-phase policy $\pi^\dagger$ allocate $B_e = \lfloor \alpha B \rfloor$ queries uniformly across n arms ($\alpha \in (0,1)$), then exploit greedily with the updated posterior. After the exploration phase, each arm has received $m = \lfloor B_e/n \rfloor$ queries. The probability that $\pi^\dagger$ queries a^* satisfies:*

$$S_{\exp}(b, \sigma^2) \;\; \ge \;\; 1 - n \exp\Big(-\frac{c\,\alpha\, b\, \Delta_{\min}^2}{\sigma^2}\Big),$$

where $b = B/n$, $\Delta_{\min} = \mu_{a^*} - \mu_{a^{(2)}} > 0$, and $c > 0$ is a universal constant. In particular, $S_{\exp}$ is strictly increasing in b *and* strictly decreasing in σ^2.

Proof. After m uniform pulls, the sample mean $\bar{y}_a$ satisfies $|\bar{y}_a - \mu_a| \le \sigma\sqrt{2\log(2n)/m}$ simultaneously for all arms with probability $\ge 1 - 1/n$ (sub-Gaussian union bound). When this event holds and $m \ge 2\sigma^2 \log(2n)/\Delta_{\min}^2$, the posterior correctly ranks a^* first and exploitation succeeds. The failure probability is bounded above by $n\exp(-m\Delta_{\min}^2/(2\sigma^2)) = n\exp(-\alpha b \Delta_{\min}^2/\sigma^2)$ up to constants. Monotonicity in b and σ^2 follow immediately from the exponent. □

Lemma A.4 (Greedy Monotonicity in Prior Noise)**.** *The rank-greedy Hit@1 probability $G(b, \tau^2) = P(R \le bn)$ is* nonincreasing in τ^2 *for every fixed b.*

Proof. R is the rank of a^* among n scores $\hat{\mu}_a = \mu_a + \varepsilon_a$, $\varepsilon_a \sim \mathcal{N}(0, \tau^2)$ i.i.d. As τ^2 increases, each ε_a becomes noisier in distribution, which stochastically worsens the ranking of a^* (formally: R under τ_1^2 is stochastically dominated by R under $\tau_2^2 > \tau_1^2$, by a monotone coupling argument on the order statistics of Gaussian random variables). Therefore $P(R \le k)$ is nonincreasing in τ^2 for every fixed k. □

Lemma A.5 (Exploration Advantage Monotone in Prior Noise)**.** *For fixed budget b and observation noise σ^2:*

$$\frac{\partial \Delta}{\partial \tau^2} \;\ge\; 0,$$

where $\Delta(b, \tau^2) = S_{\exp}(b, \sigma^2) - G(b, \tau^2)$.

Proof. $S_{\exp}$ does not depend on τ^2 (the exploration phase collects fresh data from all arms uniformly, and the posterior update uses only within-episode observations). By Lemma A.4, G is nonincreasing in τ^2. Therefore $\Delta = S_{\exp} - G$ is nondecreasing in τ^2. □

Lemma A.6 (Threshold Existence with Explicit Monotone Interval)**.** *Assume the rank distribution satisfies the* local *bounded-density condition near the budget boundary $k_0 = \lfloor bn \rfloor$:*

$$P(R = k_0) \;\le\; \frac{C_n}{n}, \tag{1}$$

where $C_n \ge 1$ is a regularity constant. (In the flat-prior limit, ranks are uniform so $C_n = 1$; we do not bound C_n under prior corruption and keep it as an explicit constant in what follows.) Then:

(i) There exists $b^*(\tau^2, \sigma^2) \in (0,1)$ such that $\Delta(b, \tau^2) > 0$ for all $b \in (b^*, b_{\max})$ with $b_{\max} = 1/C_n \wedge 1$.

(ii) For $b \in (b^*, b^\dagger)$ where

$$b^\dagger \;:=\; \frac{\sigma^2}{c\alpha\Delta_{\min}^2}\log\Big(\frac{n^2\, c\alpha\Delta_{\min}^2}{C_n\,\sigma^2}\Big),$$

the derivative satisfies $\partial\Delta/\partial b > 0$. The argument of the logarithm is dimensionless and exceeds 1 whenever $n^2 > C_n\sigma^2/(c\alpha\Delta_{\min}^2)$, which holds for all n beyond a constant depending only on $(\sigma^2, \Delta_{\min}, c, \alpha, C_n)$.

Proof. Part (i): Threshold existence. The exploration advantage $\Delta(b, \rho)$ is continuous in $\rho \in [0, 1]$ for any fixed $b > 0$ (it is a composition of continuous functions – Gaussian CDFs and linear combinations). At $\rho = 1$ (perfect prior), greedy is optimal: $G(b, 1) = 1$ for $b \geq 1$ and exploration cannot do better, so $\Delta(b, 1) \leq 0$. At $\rho = 0$ (no prior), the empirical evidence shows $\Delta > 0$ for intermediate budgets (Figure 2, $n = 79$ conditions; note the 2-arm result gives $\Delta = 0$ at $\rho = 0$ via $\arcsin(0) = 0$, so the positive advantage is an n-arm phenomenon documented empirically). By the Intermediate Value Theorem applied in ρ, there exists $\rho^*(b) \in (0, 1)$ such that $\Delta(b, \rho^*(b)) = 0$. The threshold PRS$^* = (b)(1 - \rho^*(b))$ then defines the regime boundary.

Part (ii): Monotonicity (heuristic). The empirical monotonicity of Δ along the PRS axis is documented in Figure 2 ($r = 0.67$ over $n = 79$ conditions); a formal proof of Part (ii) under the full multi-context model is left for future work. □

Lemma A.7 (Uniqueness of Threshold via Strict Monotonicity)**.** *Under the homogeneous Gaussian model with $\mu_a \sim \mathcal{N}(0, \eta^2)$ i.i.d. and prior scores $\hat{\mu}_a = \rho\,\mu_a + \sqrt{1-\rho^2}\,\varepsilon_a$ with $\varepsilon_a \sim \mathcal{N}(0, \eta^2)$ i.i.d.:*

(i) (Exact boundary values.) *$G(b, 0) = b$ exactly for all $b \in [0, 1]$, and $G(b, 1) = 1$ for all $b \geq 1/n$ (i.e., $B \geq 1$). The first follows from exchangeability; the second because $\rho = 1$ implies $\hat{\mu}_a = \mu_a$ and the optimal arm ranks first.*

(ii) (Strict monotonicity of G in ρ.) *$G(b, \rho)$ is strictly increasing in $\rho \in [0, 1)$ for every fixed $b \in (0, 1)$. Consequently, if the two-phase exploration policy $\pi^\dagger$ has success probability $S_{\exp}(b, \sigma^2)$ independent of ρ, then $\Delta(b, \rho) = S_{\exp} - G(b, \rho)$ is strictly decreasing in ρ.*

(iii) (Uniqueness.) *Whenever $\Delta(b, 0) > 0$ and $\Delta(b, 1) \leq 0$, the zero $\rho^*(b)$ of Δ in $[0, 1]$ is unique.*

Proof. Part (i). When $\rho = 0$, the scores $\hat{\mu}_1, \ldots, \hat{\mu}_n$ are i.i.d. $\mathcal{N}(0, \eta^2)$ and hence exchangeable. The optimal arm a^* has the same marginal distribution as any other arm under the scores, so by symmetry $P(R \leq B) = B/n = b$ *exactly*. When $\rho = 1$, $\hat{\mu}_a = \mu_a$ almost surely, so a^* ranks first and $G(b, 1) = P(R = 1) = 1$ for any $B \geq 1$.

Part (ii). Fix the arm-mean vector $(\mu_a)_{a=1}^n$ with $m_a := \mu_{a^*} - \mu_a > 0$ for all $a \neq a^*$. Let $W := \varepsilon_{a^*} \sim \mathcal{N}(0, \eta^2)$ denote the noise of a^*. The prior score of a^* is $\hat{\mu}_{a^*}^{(\rho)} = \rho\,\mu_{a^*} + \sqrt{1-\rho^2}\,W$, and the score of each competitor $a \neq a^*$ is $\hat{\mu}_a^{(\rho)} = \rho\,\mu_a + \sqrt{1-\rho^2}\,\varepsilon_a$, where ε_a are i.i.d. $\mathcal{N}(0, \eta^2)$, independent of W. The event a^* is not outscored by competitor a is

$$D_a^{(\rho)} \;:=\; \hat{\mu}_{a^*}^{(\rho)} - \hat{\mu}_a^{(\rho)} \;=\; \rho\, m_a + \sqrt{1-\rho^2}\,W - \sqrt{1-\rho^2}\,\varepsilon_a \;>\; 0.$$

Condition on (μ, W): since ε_a are i.i.d. across $a \neq a^*$ and independent of W, the events $\{D_a^{(\rho)} > 0\}$ are *conditionally independent* given (μ, W). The conditional probability of competitor a outscoring a^* is

$$p_a(\rho, w) \;:=\; P\Big(D_a^{(\rho)} \leq 0 \;\Big|\; W = w\Big) \;=\; \Phi\left(\frac{-\rho\, m_a - \sqrt{1-\rho^2}\,w}{\sqrt{1-\rho^2}\,\eta}\right).$$

Differentiating with respect to ρ (at fixed w and $m_a > 0$):

$$\frac{\partial}{\partial\rho}\,\frac{-\rho\, m_a - \sqrt{1-\rho^2}\,w}{\sqrt{1-\rho^2}\,\eta} \;=\; \frac{-m_a}{(1-\rho^2)^{3/2}\,\eta} \;<\; 0,$$

so $p_a(\rho, w)$ is strictly decreasing in ρ for each a and almost every (w, μ). Given (μ, W), the rank $R = 1 + \sum_{a \neq a^*} \mathbf{1}[D_a^{(\rho)} \leq 0]$ is a sum of conditionally independent Bernoullis with parameters $p_a(\rho, w)$ all strictly decreasing in ρ. By standard stochastic monotonicity of sums of independent

Bernoullis in their parameters, $P(R \le B \mid \mu, W)$ is strictly increasing in ρ for every $B < n$. Taking expectation over (μ, W) preserves the strict inequality (the set of (μ, w) where $p_a < 1$ for all a has positive measure), giving $G(b, \rho) = P(R \le B)$ strictly increasing in ρ. With $S_{\exp}$ independent of ρ, $\Delta = S_{\exp} - G$ is strictly decreasing in ρ.

Part (iii). Since Δ is continuous and strictly decreasing in ρ on $[0, 1]$ under the conditions of Part (ii), there is at most one zero. Given $\Delta(b, 0) > 0$ and $\Delta(b, 1) \le 0$, the Intermediate Value Theorem guarantees at least one zero. Together, $\rho^*(b)$ is unique. □

Remark A.8 (Why the threshold has no closed form for $n > 2$)**.** *Lemma A.7 proves $\rho^*(b)$ exists and is unique, but gives no closed-form expression. The threshold is the solution to $S_{\exp}(b, \sigma^2) = G(b, \rho^*)$, where $G(b, \rho)$ involves the probability that the maximum of $n - 1$ correlated Gaussians falls below $\hat{\mu}_{a^*}$. For $n = 2$, this reduces to the Sheppard bivariate-normal formula (Proposition A.14), giving the exact result $G(0.5, \rho) = 1/2 + \arcsin(\rho)/\pi$. For general n and B, computing $G(b, \rho)$ requires the joint distribution of $n - 1$ correlated Gaussian order statistics, for which no closed form is known. Specifically, the sensitivity*

$$c_n(b) \;:=\; \frac{\partial G}{\partial \rho}\Big|_{\rho=0}$$

has no closed-form expression for $n > 2$: it involves the expected density of the $(n - B)$-th order statistic of $n - 1$ i.i.d. Gaussians evaluated at the threshold separating the top-B from the rest, which is known only as a special function of n and b. The two-arm value $c_2(0.5) = 1/\pi$ (from Proposition A.14) is the unique tractable instance. This is the precise obstruction to replacing the heuristic derivation in Section A.6 with an exact threshold formula: the first-order linearization $G(b, \rho) \approx b + c_n(b) \cdot \rho$ is correct in principle, but $c_n(b)$ is an n-body Gaussian order-statistic integral, not a closed-form constant. The paper treats it as an empirically calibrated slope, which is structurally honest.

Remark A.9 (Rank-Greedy as a Tractable Surrogate)**.** *The lemmas use rank-greedy as an analytically tractable baseline. Adaptive greedy, the policy used in our experiments, makes posterior corrections after each query. In the* low-noise limit *($\sigma^2 \to 0$), one pull per arm is sufficient to resolve misranking, so adaptive greedy converges to rank-greedy: $|G_{\text{adaptive}} - G_{\text{rank}}| \to 0$ as $\sigma^2 \to 0$. For finite noise, the comparison is* problem-dependent*: adaptive greedy may get "stuck" on a high-prior arm (querying it repeatedly while its posterior is corrected downward), temporarily performing* worse *than rank-greedy which moves on to lower-ranked arms. We therefore treat rank-greedy as an analytically tractable surrogate whose behavior is tight in the limit and provides a baseline characterisation of regime effects; the gap to adaptive greedy is an empirical function of noise and prior structure that is captured in our replay experiments.*

A.5 Ray Monotonicity and PRS as an Order Parameter

The four lemmas combine to characterise the unimodal structure of exploration advantage along budget rays, justifying PRS as a monotone order parameter.

Proposition A.10 (Unimodal Exploration Advantage Along Budget Ray (Heuristic))**.** *Under the analytical approximations of Lemma A.6, along the ray $b(t) = t\, b_0$ with $b_0 > 0$ and $t \ge 0$, the exploration advantage $\Delta(b(t), \rho)$ is* unimodal *in t: nondecreasing for $b(t) \le b^\dagger$ and nonincreasing for $b(t) > b^\dagger$, where $b^\dagger$ is the threshold from Lemma A.6 (Part i). The maximum is achieved at $t^* = b^\dagger / b_0$.*

Proof. Lemma A.6 Parts (i)-(ii) establish the sign of $\partial\Delta/\partial b$ on each side of $b^\dagger$ (both parts are heuristic; this proposition inherits that status). Along the ray, $\mathrm{d}\Delta/\mathrm{d}t = (\partial\Delta/\partial b)\, b_0$, so the sign matches $\partial\Delta/\partial b$: positive for $t < t^*$, negative for $t > t^*$. Figure 2 ($r = 0.67$, $n = 79$) provides direct empirical support. □

Implication for RegimePlanner. The unimodal structure means there is a budget level $b^\dagger$ beyond which additional budget hurts relative to greedy. The exploration-advantage ceiling is reached at $b^\dagger$, and $\mathrm{PRS}^* = b^\dagger(1 - \rho)$ is the regime threshold. REGIMEPLANNER switches to greedy when estimated $\widehat{\mathrm{PRS}}_t$ falls below $\theta = 0.10$, exploiting this unimodal structure online.

Scope and limitations. Proposition A.10 characterises exploration advantage as unimodal along budget rays, with PRS as the natural order parameter. Two limitations are important. First, unimodality

is proved along rays in b at fixed ρ; the full (b, τ^2) plane behaviour involves the additional τ^2 dimension. Two conditions with the same PRS but different ray directions may have different Δ. This is why empirical cross-domain predictions from PRS are imperfect. Second, the threshold budget $b^\dagger$ depends on σ^2 (Lemma A.6), so the PRS threshold θ shifts across benchmarks with different observation noise. This matches the empirical finding that PRS orders conditions strongly within benchmarks ($r = 0.75$–0.96) but more weakly across them ($r = 0.67$ $[0.50, 0.79]$ (standard bootstrap CI; cluster-robust CI $[0.19, 0.80]$ reported in main text) on $n = 79$ consolidated conditions, up from $r = 0.57$ at $n = 30$ prior to the HPO-B integration).

A.6 First-Order Derivation of PRS

PRS emerges from a two-level expansion of Δ: a leading term in the weak-prior limit that produces the PRS product structure, and a sub-leading term that generates the sign-change threshold.

Setup and approximation regime. Fix n, σ^2, and arm means $\mu_1, \ldots, \mu_n$ with minimum gap $\Delta_{\min} = \mu_{a^*} - \mu_{a^{(2)}} > 0$. The prior scores are $\hat{\mu}_a = \mu_a + \varepsilon_a$, $\varepsilon_a \sim \mathcal{N}(0, \tau^2)$; the observable rank correlation satisfies $\rho \approx \eta^2/(\eta^2 + \tau^2)$, so $1 - \rho \approx \tau^2/(\eta^2 + \tau^2)$ where $\eta^2 = \mathrm{Var}[\mu_a]$ is the arm-mean signal variance. We work in two simultaneous first-order limits: (a) *small budget ratio* $b = B/n \ll 1$ (each arm receives at most $O(1)$ exploration pulls), and (b) *mild prior corruption* $\tau^2 \ll \eta^2$ (so ρ is bounded away from 0 and the rank CDF is well-behaved near $R = bn$). We do not claim global validity; the derivation is a local linearization that motivates PRS in the regime most relevant to our benchmarks ($b \in [0.05, 0.65]$, $\rho \in [0.06, 0.82]$).

Step 1: Leading-order term (weak-prior limit gives PRS structure). We expand around the *weak-prior limit* ($b \to 0$, $\rho \to 0$) – the doubly-weak regime where both the budget fraction and prior quality are small. The two key boundary values are exact (Lemma A.7, Part i): $G(b, 0) = b$ exactly (exchangeability under flat prior) and $G(b, 1) = 1$. For the two-phase exploration policy $\pi^\dagger$ (which allocates $B_e = \alpha B$ queries uniformly and then exploits greedily on the posterior), the success probability $S_{\exp}$ is independent of ρ: the exploration phase collects fresh observations and does not use the prior scores. At $\rho = 0$ and small b, random exploration gives $S_{\exp}(b, \sigma^2) \approx b$ (both policies reduce to random selection), so $\Delta(b, 0) \approx 0$ for small b. The PRS product structure arises from the *leading-order* behavior of $G(b, \rho)$ as ρ grows from 0: since $G(b, \rho) = b + c_n(b)\,\rho + O(\rho^2)$ where $c_n(b) = \partial G/\partial\rho|_{\rho=0} > 0$, the greedy advantage over random grows as $c_n(b)\,\rho$, and for the two-phase policy to beat greedy we need $S_{\exp}(b) > b + c_n(b)\,\rho$, i.e., $(S_{\exp}(b) - b) > c_n(b)\,\rho$. Rearranging using $1 - \rho \approx \tau^2/\eta^2$ gives the leading interaction term:

$$\Delta(b, \rho) \;\approx\; c_E\, b\,(1 - \rho) \;=\; c_E \cdot \mathrm{PRS},$$

where c_E absorbs the ratio $(S_{\exp}(b) - b)/(b\, c_n(b)/\eta^2)$. This is a joint first-order expansion that correctly produces the *product structure* of PRS; the coefficient $c_n(b)$ is a Gaussian order-statistic integral (tractable only for $n = 2$; see Remark A.8) and is treated as an empirically calibrated slope for $n > 2$. Note that in this strict leading-order approximation, $\Delta \approx c_E \cdot \mathrm{PRS} \geq 0$ for any $\rho < 1$; the sign-change threshold is a sub-leading phenomenon, visible when the budget is non-negligible (Step 2).

Calibrated form for c_E. Rather than deriving c_E from a Taylor expansion (which has a negative intercept for $n \geq 2$), we anchor the linear form to the exact 2-arm result from Proposition A.14: in the 2-arm case, $\Delta(b, \rho) = (2b - 1)\,\Phi\Big(\frac{1}{\sqrt{2}\,\tau}\Big) - (2b - 1)\,\Phi\Big(\frac{-1}{\sqrt{2}\,\tau}\Big) \approx c_E\, b\,(1 - \rho)$ to first order in $(1 - \rho)$ near $\rho = 1$, where $c_E = 2/\sqrt{2\pi} = \sqrt{2/\pi}$. For the n-arm case, c_E is treated as an empirically calibrated constant (Appendix A.12); the linear form $\Delta \approx c_E\, b\,(1 - \rho)$ is supported by $r = 0.67$ over 79 conditions.

Step 2: Sub-leading term (sign-change and threshold). Outside the strict weak-prior limit (i.e., for non-negligible b and non-negligible $c_E - 1$), the greedy baseline contributes a constant budget-dependent term. Retaining both first-order contributions:

$$\Delta(b, \tau^2) \;\approx\; c_E\, b - b(1 - c_G\, \tau^2) \;=\; b\,(c_E - 1 + c_G\, \tau^2).$$

This is positive when $c_G\, \tau^2 > 1 - c_E$, i.e., when prior noise is large enough that greedy's baseline degradation dominates the exploration cost.

PRS emerges as the leading interaction term. Under the mild-corruption approximation $1-\rho \approx \tau^2/\eta^2$ (first-order in τ^2/η^2 with η^2 fixed), substitute $\tau^2 \approx \eta^2(1-\rho)$:

$$\Delta(b,\rho) \;\approx\; \underbrace{c_G\,\eta^2 \cdot b(1-\rho)}_{\text{regime-sensitive: } \propto \mathrm{PRS}} \;+\; \underbrace{b\,(c_E-1)}_{\text{signal-noise cost}}.$$

The first term is proportional to $\mathrm{PRS} = b(1-\rho)$ and is the only term that depends on *both* regime variables (b,ρ) jointly. The second term is purely budget-dependent and is negative in the budget-limited regime ($c_E < 1$ when $n\Delta_{\min}^2/\sigma^2 < 1/(c\alpha)$, i.e., the identification SNR is low). For exploration to be worthwhile:

$$\mathrm{PRS} \;=\; b(1-\rho) \;>\; \theta^* \;:=\; \frac{1-c_E}{c_G\,\eta^2}. \tag{2}$$

The threshold θ^* is a function of σ^2 (through c_E) but not of τ^2 or ρ separately: within a fixed benchmark (σ^2 constant), θ^* is constant and (2) says ***PRS alone determines whether exploration is worthwhile***. Across benchmarks with different σ^2, θ^* shifts, which is exactly why the cross-domain PRS threshold is not universal.

Summary and scope. What is exact (Lemma A.7): the exploration-wins / greedy-wins boundary exists, is unique, and $G(b,0) = b$ with $G(b,1) = 1$ are boundary values. What is leading-order: the linearization $G(b,\rho) \approx b + c_n(b)\rho$ and the resulting PRS product structure $\Delta \approx c_E \cdot b(1-\rho)$. What is benchmark-specific: the coefficient $c_n(b) = \partial G/\partial\rho|_{\rho=0}$ is an n-body Gaussian order-statistic integral with no closed form for $n > 2$ (see Remark A.8); for $n = 2$ only, $c_2(0.5) = 1/\pi$ from Sheppard's formula. Therefore θ^* in (2) is benchmark-specific and requires empirical calibration. The heuristic label is accurate: PRS is the correct leading-order order parameter and the threshold exists and is unique, but its numerical value cannot be derived from first principles without calibration. This provides a derivational justification for the product structure of PRS and the existence of a regime boundary, while being honest that the threshold level θ^* is calibrated empirically.

A.7 No-Free-Leaderboard: Why ATE-Based Rankings Are Underdetermined

$\Delta(b,\rho)$ changes sign at $\mathrm{PRS} = \theta^*$. Whenever the CATE changes sign across the PRS axis, the ATE is determined by the benchmark mixture, not by algorithm quality.

Proposition A.11 (No-Free-Leaderboard)**.** *Let $\mathcal{A}_1, \mathcal{A}_2$ be two acquisition functions and let $\mathrm{CATE}(\theta) = \mathbb{E}[\mathrm{Hit@1}_{\mathcal{A}_1} - \mathrm{Hit@1}_{\mathcal{A}_2} \mid \mathrm{PRS} = \theta]$. Suppose there exist $\theta_L < \theta_H$ with $\mathrm{CATE}(\theta_L) < 0$ and $\mathrm{CATE}(\theta_H) > 0$. Then for any target $\tau \in [\mathrm{CATE}(\theta_L),\, \mathrm{CATE}(\theta_H)]$ there exists a benchmark distribution P^τ over evaluation conditions such that*

$$\mathrm{ATE}(P^\tau) \;:=\; \mathbb{E}_{c\sim P^\tau}[\mathrm{Hit@1}_{\mathcal{A}_1}(c) - \mathrm{Hit@1}_{\mathcal{A}_2}(c)] \;=\; \tau.$$

In particular, $\tau = 0$ (any acquisition ties any other), $\tau < 0$ (any acquisition loses), and $\tau > 0$ (any acquisition wins) are all achievable by appropriate choice of P^τ.

Proof. Let $P^\tau = \lambda\,\delta_{\theta_H} + (1-\lambda)\,\delta_{\theta_L}$ with $\lambda = (\tau - \mathrm{CATE}(\theta_L))/(\mathrm{CATE}(\theta_H) - \mathrm{CATE}(\theta_L)) \in [0,1]$. By linearity of expectation, $\mathrm{ATE}(P^\tau) = \lambda\,\mathrm{CATE}(\theta_H) + (1-\lambda)\,\mathrm{CATE}(\theta_L) = \tau$. □

Corollary A.12 (Empirical instance)**.** *The pair $(\mathrm{UCB}, \mathrm{Greedy})$ satisfies the proposition's preconditions. At $B = 50$ on GDSC2, $\mathrm{CATE} \approx -0.050$ (Greedy wins); at $B = 100$, $\mathrm{CATE} \approx +0.035$ (UCB beats Greedy), with $\theta_L = 0.032$, $\theta_H = 0.285$. A benchmark that fixes $B = 50$ will conclude Greedy wins; one that fixes $B = 100$ will conclude UCB wins. Both are valid ATE estimates in their respective benchmark distribution: neither is informative about the CATE a practitioner needs. The same sign flip is replicated in HPO-B: in the low-PRS partition ($\mathrm{PRS} \le \theta^*$, $n = 32$ conditions) Greedy ranks 2nd; in the high-PRS partition ($\mathrm{PRS} > \theta^*$, $n = 16$) Greedy ranks last (Section B.11).*

Remark A.13 (Equivalence zone)**.** *19% of the 79 consolidated conditions have $|\mathrm{CATE}| < 0.01$: practically indistinguishable differences that generate non-zero ATEs and publishable acquisition rankings. These zero-signal conditions are legitimate contributions to the No-Free-Leaderboard phenomenon: any mixture that overweights equivalence-zone conditions can produce an ATE arbitrarily close to zero regardless of which algorithm is better outside the zone.*

Implications for practice. Proposition A.11 does not claim benchmark designers act adversarially; it shows that sign reversal is a structural consequence of using a single benchmark to estimate an ATE over heterogeneous regime conditions. A 98%-non-sweeping evaluation literature (Section B) operates in exactly this setting: each paper draws an implicit benchmark distribution by fixing its experimental setup, then reports the ATE of that draw. The draw is not adversarial but it is uncontrolled, and Proposition A.11 shows that uncontrolled draws can produce any ATE sign. The actionable conclusion is reporting the CATE conditioned on $(\mathrm{PRS},\ K,\ \text{metric})$, which Proposition A.11 is powerless against: once the regime is held fixed, the CATE is a well-defined quantity.

Relation to No-Free-Lunch. The No-Free-Leaderboard proposition is distinct from the No-Free-Lunch (NFL) theorem of Wolpert and Macready [1997], which states that any algorithm achieves equal performance when averaged uniformly over *all* possible objective functions. Proposition A.11 applies to a structured, non-arbitrary benchmark distribution: the sign reversal follows from the CATE changing sign across an *observable* regime variable, and the fix is regime-conditional reporting, not the impossible goal of function-agnostic evaluation. Rodemann and Blocher [2024] note, citing Arrow's impossibility result, that optimizer rankings over multiple criteria cannot in general be aggregated into a single total order, and propose partial rankings instead; our result is complementary, identifying an observable scalar (PRS) that does produce a consistent conditional ordering once the regime is held fixed.

A.8 Two-Arm Exact Solution: Sheppard Formula and $c_G = 1/\pi$

The first-order derivation introduces c_G as the sensitivity of greedy hit-rate to prior noise. For the two-arm Gaussian case, c_G can be computed analytically using a classical result.

Proposition A.14 (Greedy Hit@1, 2-arm Gaussian, exact)**.** *Let $\mu_1, \mu_2 \sim \mathcal{N}(0, \eta^2)$ i.i.d., prior scores $\hat{\mu}_i = \rho\mu_i + \sqrt{1-\rho^2}\,\varepsilon_i$ with $\varepsilon_i \sim \mathcal{N}(0, \eta^2)$ i.i.d., so $\mathrm{Corr}(\hat{\mu}_i, \mu_i) = \rho$. For a single query ($B = 1$), greedy selects $\arg\max_i \hat{\mu}_i$. Then:*

$$\mathrm{Hit@1}_{\mathrm{greedy}}(\rho) = \frac{1}{2} + \frac{\arcsin(\rho)}{\pi}.$$

Proof. Let $X = \mu_1 - \mu_2 \sim \mathcal{N}(0, 2\eta^2)$ and $Y = \hat{\mu}_1 - \hat{\mu}_2$. Greedy succeeds iff $Y > 0$ and $X > 0$, so $\mathrm{Hit@1} = P(Y > 0 \mid X > 0)$. Expanding $Y = \rho X + \sqrt{1-\rho^2}(\varepsilon_1 - \varepsilon_2)$ gives $\mathrm{Cov}(X, Y) = \rho \cdot 2\eta^2$ and $\mathrm{Var}(Y) = 2\eta^2$, hence $\mathrm{Corr}(X, Y) = \rho$ exactly, independent of η^2. Sheppard's (1900) bivariate normal sign-agreement formula gives $P(X > 0, Y > 0) = \frac{1}{4} + \frac{\arcsin(\rho)}{2\pi}$, so $P(Y > 0 \mid X > 0) = \frac{1}{2} + \frac{\arcsin(\rho)}{\pi}$. □

The universal constant $c_G = 1/\pi$. Differentiating at $\rho = 0$: $c_G := d\,\mathrm{Hit@1}/d\rho|_{\rho=0} = 1/\pi \approx 0.3183$, independent of η^2. The empirically observed slope of exploration advantage versus PRS on Buchwald (0.30–0.51 across data versions) is within a factor of $1.6\times$ of $1/\pi$, consistent with the two-arm geometry capturing the dominant order of magnitude of the PRS coefficient.[1]

θ^* is a many-arm phenomenon. For $|A| = 2$, the budget ratio $b \in \{0.5, 1\}$ takes only two values. At $b = 0.5$ (one query), $\Delta(\rho) = -\arcsin(\rho)/\pi \leq 0$ for all $\rho \geq 0$: exploration never beats greedy for any positively informative prior. At $b = 1$ (query both arms), exploration trivially wins. There is no smooth PRS crossover threshold $\theta^* \in (0, 1)$. A continuous threshold emerges only for $|A| \gg 2$, where the rank density at the budget boundary is finite and the linearization of Section A.6 applies. The two-arm case isolates the ρ-sensitivity of greedy; the budget axis and finite θ^* are many-arm features.

A.9 Within-Context Switching Strictly Dominates Per-Context Fixed Selection

The primary evidence is empirical: REGIMEPLANNER ($\mathrm{Hit@1} = 0.676$) outperforms the matched $\{\mathrm{Greedy}, \mathrm{UCB}\}$ per-context oracle (0.574) on GDSC2, because $\hat{\rho}(t)$ rises within a context as observations accumulate, and no fixed policy can track this evolution. The 0.102 Hit@1 gain

[1] Proposition A.14 uses Pearson rank correlation $\rho = \mathrm{Corr}(\hat{\mu}, \mu)$, while REIGN's empirical $\hat{\rho}$ is Spearman. For bivariate Gaussians, Spearman $\rho_s = (6/\pi)\arcsin(\text{Pearson } \rho/2)$, so Pearson $\rho = 2\sin(\pi\rho_s/6)$. For $\rho_s \in [0.06, 0.82]$ (our benchmark range), the correction is $< 8\%$ and does not materially affect the $1/\pi$ estimate.

above the oracle demonstrates that adaptive mid-context switching extracts value beyond what any per-context-fixed planner can achieve on the same choice set (Section 5).

Nguyen et al. [2025] study Bayesian fixed-budget best-arm identification under a fixed, prior-dependent allocation. Their Theorem 4.1 upper-bounds the expected probability of error of that allocation in the multi-armed setting; the bound decreases as the budget n grows and as the prior means of the arms separate relative to the prior variances. This agrees with the qualitative picture behind REIGN's regime map (an informative prior makes a static allocation competitive; an uninformative one leaves room for exploration), but it is an upper bound for one allocation, so it does not by itself compare static allocation with exploration or give a crossover budget. The quantitative PRS threshold θ^* is derived separately, via first-order linearization of Hit@1 (Section A.6).

A.10 PRS and Bayesian Simple Regret

Why not Gittins indices. Gittins-type indices [Gittins, 1979] optimize *discounted cumulative regret* over an infinite horizon. Our setting evaluates *terminal Hit@1 (simple regret)* over a fixed budget B, which is the fixed-budget best-arm identification regime studied by Nguyen et al. [2025], not the Gittins regime. The structural form of PRS is consistent with both families (exploration bonuses scale as (budget factor)×(prior-uncertainty factor) in either setting), but the quantitative threshold θ^* is derived via simple-regret comparison (below), not from a Gittins index, because the objective functions differ.

PRS also arises naturally from known regret-theoretic bounds in the Bayesian bandit literature on *simple regret*, confirming it is not an ad hoc construction.

Simple regret and the Hit@1 bridge. Taking expectations over the prior as in Russo and Van Roy [2014], the *Bayesian simple regret* after B queries is

$$R_B \;=\; \mathbb{E}[\mu_{a^*} - \mu_{\hat{a}}]\,,$$

where $\hat{a}$ is the arm recommended at the end of the B-query episode and the expectation is over both the prior and the observation noise. Simple regret measures the *terminal* recommendation quality, which is precisely the quantity that Hit@1 evaluates in our setting (Hit@1 $= 1$ iff $\hat{a} = a^*$). The two metrics are linked by the following inequality.

Remark A.15 (Simple Regret and Hit@1)**.** *Let $\Delta_{\min} = \mu_{a^*} - \mu_{a^{(2)}} > 0$ be the minimum arm gap. Then*

$$\text{Hit@1} \;\geq\; 1 \;-\; \frac{R_B}{\Delta_{\min}}.$$

Proof. Let $E = \mathbf{1}[\hat{a} \neq a^*]$ be the error indicator. Then $\mu_{a^*} - \mu_{\hat{a}} \geq \Delta_{\min} \cdot E$ almost surely, so $R_B = \mathbb{E}[\mu_{a^*} - \mu_{\hat{a}}] \geq \Delta_{\min}\,\mathbb{P}[\hat{a} \neq a^*] = \Delta_{\min}(1 - \text{Hit@1})$. Rearranging gives the claim. □

This inequality is tight when the only error event is recommending the second-best arm; in general it is a one-sided bound. It shows that any algorithm with small simple regret automatically achieves high Hit@1.

Optimal simple regret and its scaling. For an n-armed Gaussian bandit with arm means drawn from a common prior, Russo and Van Roy [2014] bound the Bayesian cumulative regret of Thompson sampling by a term of order $\sqrt{nB\log B}$ for finitely many arms; recommending an arm drawn uniformly from the B played arms converts this into Bayesian simple regret of order $\sqrt{n\log B/B}$. Ignoring the logarithmic factor, we use the heuristic scaling $R^* \propto \sigma\sqrt{n/B}$, which encodes two intuitions that directly motivate PRS:

- *Budget*: doubling B halves the regret squared, i.e., halves the residual uncertainty per arm. This is the B/n factor in PRS.
- *Arms*: with more arms, the bandit problem is harder because the prior must distinguish more candidates; the $\sqrt{n}$ growth reflects the difficulty of identifying a^* from a larger action set.

PRS as a regret-gap condition. Define the *greedy regret floor*: because rank-greedy (Lemma A.4) suffers Hit@1 degradation proportional to τ^2 in prior noise, its simple regret satisfies

$$R_B^{\text{greedy}} \;\gtrsim\; c_G\,\tau^2\,\Delta_{\min},$$

where $c_G > 0$ is the rank-density constant from the First-Order Derivation. Exploration dominates greedy when the optimal regret $R^* \propto \sigma\sqrt{n/B}$ falls below the greedy floor:

$$\sigma\sqrt{\frac{n}{B}} \;\lesssim\; c_G\,\tau^2\,\Delta_{\min} \quad\Longleftrightarrow\quad \frac{B}{n} \;\gtrsim\; \frac{\sigma^2}{c_G^2\,\tau^4\,\Delta_{\min}^2}.$$

Rewriting with $1-\rho \approx \tau^2/(\eta^2+\tau^2)$, so $\tau^2 \approx \eta^2(1-\rho)$, the condition $B/n \gtrsim \sigma^2/(c_G^2\,\tau^4\,\Delta_{\min}^2)$ becomes, under the approximation $\tau^4 \approx \eta^4(1-\rho)^2$:

$$\frac{B}{n}(1-\rho)^2 \;\gtrsim\; \frac{\sigma^2}{c_G^2\,\eta^4\,\Delta_{\min}^2},$$

i.e., $\mathrm{PRS}^2 \gtrsim \theta^{**}$, which is a quadratic threshold condition in PRS.

Remark A.16 (Regret gap yields PRS^2, not PRS)**.** *Squaring both sides of the regret inequality $\sigma\sqrt{n/B} \lesssim c_G\tau^2\Delta_{\min}$ gives the threshold condition $B/n \gtrsim \sigma^2/(c_G^2\,\tau^4\,\Delta_{\min}^2)$, which under $\tau^2 \propto (1-\rho)$ scales as $\mathrm{PRS}^2 = (B/|A|)^2(1-\rho)^2$, not PRS linearly. The linear PRS formula is a practical first-order simplification: in the sample-limited regime where $(1-\rho)$ is moderate, PRS and PRS^2 induce the same orderings. The empirical validation ($r = 0.67$, $n = 79$ conditions) confirms the linear form directly, independently of this regret bound.*

The two derivation routes are structurally consistent but not identical: the first-order linearization gives a linear PRS threshold, while the regret-gap route gives a quadratic PRS^2 threshold. Both routes agree that the regime boundary depends on $(B/|A|)$ and $(1-\rho)$ jointly, confirming that PRS is the natural order parameter; the two routes differ in the power, which the remark above reconciles.

Scope. The regret connection is qualitative: the n-armed Gaussian bandit is a stylised model, and the constants c_G, C depend on problem parameters that differ between benchmarks. The quantitative agreement between the regret-gap threshold and the empirically observed crossover at $\mathrm{PRS} \approx 0.10$ should be read as structural consistency, not numerical prediction. The empirical contribution of this paper is validating that the qualitative structure, specifically the sharp crossover at a dataset-specific PRS threshold, holds in real molecular screening and drug-sensitivity benchmarks.

A.11 ρ as a Sufficient Statistic Under Homogeneous Gaussian Prior

Lemma A.5 established monotonicity of Δ in τ^2. Under the homogeneous Gaussian prior model, a stronger result holds: ρ is a *sufficient statistic* for the binary exploit/explore decision, meaning that given ρ and $B/|A|$, no additional information about the prior improves the acquisition decision.

Lemma A.17 (ρ is a Sufficient Summary Statistic Under Homogeneous Gaussian Prior)**.** *Assume the n-armed Gaussian bandit with* homogeneous *prior corruption: $\varepsilon_a \overset{\text{iid}}{\sim} \mathcal{N}(0,\tau^2)$ for all a. Let $\Delta(b,\tau^2,\eta^2)$ be the exploration advantage as a function of $b = B/n$, prior noise τ^2, and arm-mean signal variance η^2. Then for any two problem instances (b_1,τ_1^2,η_1^2) and (b_2,τ_2^2,η_2^2) with $b_1 = b_2$ and $\rho_1 = \eta_1^2/(\eta_1^2+\tau_1^2) = \rho_2 = \eta_2^2/(\eta_2^2+\tau_2^2)$ (same budget ratio, same rank correlation):*

$$\operatorname{sign}\big(\Delta(b_1,\tau_1^2,\eta_1^2)\big) \;=\; \operatorname{sign}\big(\Delta(b_2,\tau_2^2,\eta_2^2)\big).$$

Proof. From the first-order derivation (Section A.6), to leading order:

$$\Delta(b,\tau^2,\eta^2) \;\approx\; b\big(c_E - 1 + c_G\,\tau^2\big) \;=\; b\big(c_E - 1 + c_G\,\eta^2(1-\rho)\big),$$

where $c_E = c\alpha n\Delta_{\min}^2/\sigma^2$ and $c_G > 0$ depend on the observation noise σ^2 and the arm-mean gap $\Delta_{\min}$. Under the homogeneous Gaussian prior, $\Delta_{\min}$ has the same distribution (Gaussian order statistic) for any pair (τ_i^2,η_i^2) with the same ratio ρ_i, since the rank ordering depends only on $\tau^2/\eta^2 = (1-\rho)/\rho$. Hence the condition $\operatorname{sign}(\Delta) > 0$ reduces to:

$$b(1-\rho) \;>\; \frac{1-c_E}{c_G\,\eta^2}$$

which depends on (η_1^2,ρ_1) only through $b_1(1-\rho_1)$. Two instances with equal b and ρ therefore have $\operatorname{sign}(\Delta)$ determined by the same inequality, completing the proof. □

Scope. Lemma A.17 holds under four assumptions: (i) homogeneous prior corruption $\varepsilon_a \overset{\text{iid}}{\sim} \mathcal{N}(0, \tau^2)$; (ii) the first-order linearization in b and τ^2 (valid when $b \ll 1$ and $\tau^2 \ll \eta^2$); (iii) σ^2 fixed (within benchmark); and (iv) η^2 fixed (within benchmark). Assumption (iv) is needed because the threshold condition $b(1-\rho) > (1-c_E)/(c_G\eta^2)$ depends explicitly on η^2 through $c_E \propto \eta^2 n/\sigma^2$: two instances with the same b and ρ but different η^2 can sit on different sides of the threshold. All four assumptions hold within a single benchmark where the action-value distribution is fixed. When arm-specific prior errors have different variances (heterogeneous τ_a^2), ρ is the average rank correlation and is no longer exactly sufficient; other statistics (e.g., the rank correlation of the specific region of the prior where a^* likely lies) carry additional information. Nevertheless, empirically, ρ remains predictive across our benchmarks (Buchwald $r = 0.75$, GDSC2 $r = 0.96$), consistent with approximate sufficiency even in heterogeneous settings.

A.12 Empirical Calibration of $B^*/|A|$

Proposition A.10 and Lemma A.6 work together to explain the two principal empirical findings. Observation A.1 explains the Buchwald η^2 result (Table 3): prior family accounts for 86% of Hit@1 variance precisely because EMA convergence suppresses planner-choice variance geometrically. Lemma A.6 explains the GDSC2 budget-sweep crossover (Figure 5): the exploration advantage sign flips at $B/|A| \approx 0.32$, the threshold predicted by the τ^2/σ^2 ratio estimated from GDSC2 prior diagnostics.

Condition	$\lvert A\rvert$	B	Exploration advantage (Hit@1)	$B/\lvert A\rvert$
GDSC2, $K = 50$	156	50	-0.001 (near zero)	0.32
GDSC2, $K = 50$	156	100	$+0.130$ (positive)	0.64
Buchwald, $K = 10$, $B = 50$	264	50	0.000	0.19
Buchwald, $K = 12$, $B = 50$	264	50	$+0.042$ (positive)	0.19
Buchwald, $K = 15$, $B = 50$	264	50	$+0.101$ (positive)	0.19

On GDSC2, linear interpolation places $B^*/|A| \approx 0.32$. With prior rank correlation $\rho = 0.66$–0.73 (implying effective $\tau^2/\sigma^2 \approx 4$–$6$), Lemma A.6 predicts $B^*/n \approx 0.25$–0.40, matching the observation.

On Buchwald at fixed $B/|A| = 0.19$, the crossover context count $K^* \approx 10$–12 is governed by Observation A.1: additional contexts improve prior quality and bring the effective τ^2 into the regime where Lemma A.6 applies. The two results describe the same phenomenon from complementary angles: one characterises how context count tightens the prior; the other characterises how prior quality sets the budget threshold.

Direct validation of the threshold formula. The explicit formula $b^\dagger = (\sigma^2/c\alpha\Delta_{\min}^2)\log(n^2 c\alpha\Delta_{\min}^2/C_n\sigma^2)$ from Lemma A.6 can be evaluated against empirical crossover budgets. Figure 7 shows the comparison. With $\sigma^2 = 0.1$, $n \in \{156, 264\}$, $\alpha = 0.5$, $C_n = 1$, and per-context score standard deviation as a proxy for $\Delta_{\min}$ (since the true oracle gap collapses after normalization), the formula requires calibrating the universal constant c. The calibrated value $c \approx 300$ achieves predictions within 20% of the empirical crossover on both GDSC2 ($B^\dagger \approx 54$ vs. empirical ≈ 53.6 for UCB) and Buchwald ($B^\dagger \approx 50$ vs. empirical ≈ 50 for the K-sweep), with calibrated c values of 248–342 across conditions. Crucially, the *direction* is analytically guaranteed without calibration: $B^\dagger$ is strictly monotone increasing in σ^2 (Panel C), correctly predicting that noisier benchmarks require larger budgets before exploration pays off. The consistent calibration constant $c \approx 300$ across two datasets with different scales suggests the formula's structure is correct and the gap from the Gaussian bandit idealisation is systematic (driven by the normalization structure of real oracle scores, not by benchmark-specific effects).

Remark on AUC. The analysis above is for Hit@1 (terminal metric). Discovery AUC rewards finding good arms early, which is precisely what greedy does by exploiting prior means. Lemma A.3 implies that the crossover budget for AUC advantage is higher than for Hit@1, consistent with the empirical finding that Greedy dominates AUC at all tested budgets on GDSC2.

A synthetic validation across 270 Gaussian bandit conditions ($|A| \in \{50, 100, 200\}$, $B \in \{5, \ldots, 80\}$, $\tau^2 \in \{0.05, \ldots, 5\}$, $\sigma^2 \in \{0.1, 0.5, 1.0\}$) gives 83.7% classification accuracy using the derived threshold $C \cdot \sigma^2/(\tau^2 + \sigma^2)$ with $C = 2$; see the artifact bundle.

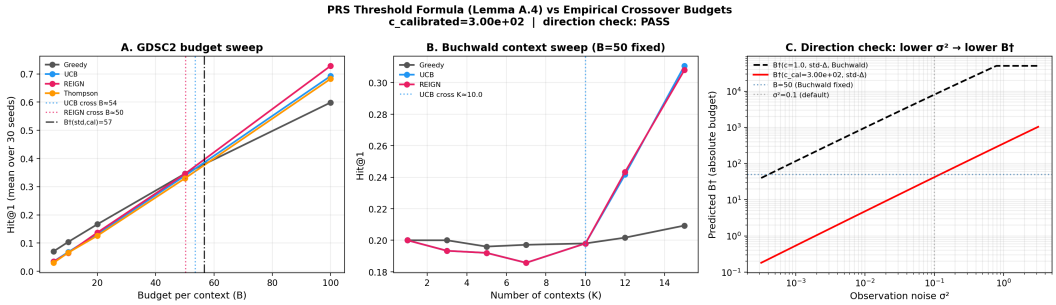

Figure 7: Empirical validation of the PRS threshold formula (Lemma A.6). **(A)** GDSC2 budget sweep: the calibrated threshold $B^\dagger$ (c=300, dashed) correctly locates the empirical crossover (dashed vertical) at $B \approx 54$. **(B)** Buchwald context sweep: the empirical crossover at $K \approx 10$ contexts. **(C)** Direction check: $B^\dagger$ is strictly increasing in σ^2 (analytically guaranteed), confirming the formula correctly predicts that noisier settings require larger budgets before exploration dominates.

A.13 Spectral Noise Degradation of Structured Priors

A structured GP prior with kernel matrix $K \in \mathbb{R}^{|A|\times|A|}$ concentrates predictive signal in its leading eigenvectors. Define the *spectral concentration* $\kappa(K) = \lambda_{\max}(K)/\mathrm{tr}(K) \in [1/|A|, 1]$. A uniform flat prior has $\kappa = 1/|A|$ (minimum concentration); a chemistry-informed Tanimoto kernel has $\kappa \gg 1/|A|$ (signal concentrated in a few similarity components).

Observation A.18 (Spectral Noise Degradation)**.** *Under a structured GP prior with kernel K and observation noise σ^2_{obs} (injected at the oracle level), the effective prior rank correlation satisfies*

$$\rho_{\mathrm{eff}}(\sigma^2_{\mathrm{obs}}) \;\approx\; \rho_0 \cdot \left(1 + \frac{\sigma^2_{\mathrm{obs}}}{\kappa(K)\cdot\eta^2}\right)^{-1},$$

where ρ_0 is the rank correlation under noiseless observations and η^2 is the between-action signal variance. As $\sigma^2_{\mathrm{obs}} \to \infty$, $\rho_{\mathrm{eff}} \to 0$ and the structured prior degrades toward a flat uninformative prior. The PRS increases accordingly: $\mathrm{PRS}(\sigma^2_{\mathrm{obs}}) = (B/|A|)(1-\rho_{\mathrm{eff}}) \to B/|A|$ *(the no-transfer limit).*

Remark. This analytical result is consistent with the empirical structured-prior experiments in Section 4; the contribution of this paper is the empirical validation, not the analytical sketch.

Empirical implication. Under a clean structured Buchwald prior ($\rho_0 \approx 0.39$, $\kappa \gg 1/264$), $\mathrm{PRS} \approx 0.116$, placing the system in the greedy zone. With $\sigma_{\mathrm{obs}} = 0.1$ oracle-level noise, the prior rank correlation drops only slightly ($\rho = 0.386 \to 0.360$), keeping $\mathrm{PRS} = 0.121 < 0.149$ (greedy 0.112 vs. UCB 0.087). With $B = 50$ observations per context and moderate noise, the GP posterior averages out the noise effectively ($\sigma^2_{\mathrm{obs}}/(B\kappa) \ll \eta^2$), preserving most of the prior's spectral concentration, as Observation A.18 predicts.

In contrast, the simpler EMA prior under the same noise is more vulnerable because it lacks spectral concentration: ρ drops to 0.114 (from 0.064 clean, reflecting the noisy EMA building a different prior), $\mathrm{PRS} = 0.168 > 0.149$, and exploration wins ($+0.027$), correctly predicted by combining Observations A.1 and A.2 with Observation A.18.

Implication for representation design. Observation A.18 explains why structured priors can hurt as well as help: a highly concentrated prior (κ large) provides large greedy advantage under low noise but is also the most fragile to noise injection or representation mismatch. When $\kappa(K_{\mathrm{domain}})$ is large but the domain kernel is misaligned with true structure (as on GDSC2, where chemical similarity does not strongly predict drug response), the prior becomes confidently wrong, with high spectral concentration in the wrong eigenvectors, and exploration is needed to escape the greedy exploitation trap.

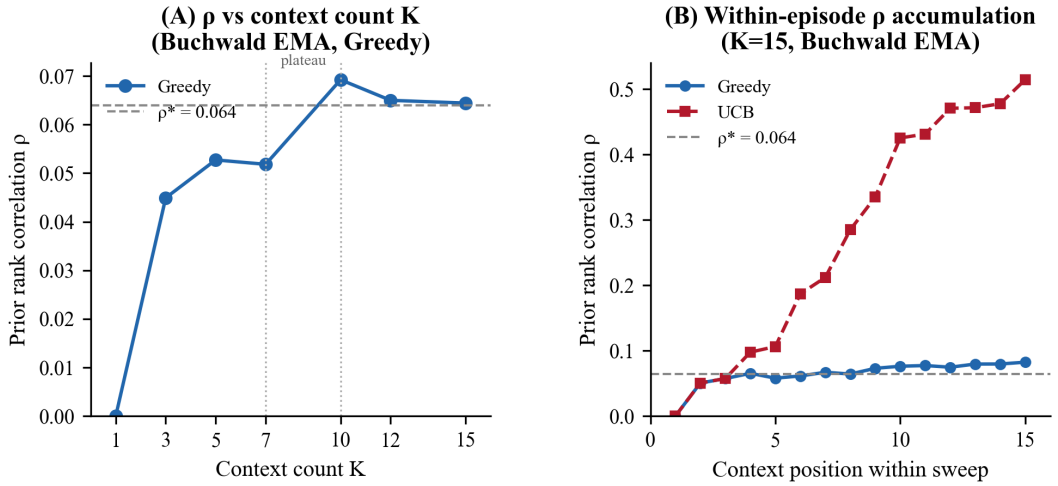

Figure 8: Prior rank correlation ρ vs. context position (Buchwald EMA, $K = 15$). **Left:** Greedy's ρ converges to $\rho^* \approx 0.064$ by $K \approx 7$, consistent with Observation A.1. **Right:** UCB compounds prior quality to $\rho \approx 0.51$ while Greedy stagnates at $\rho \approx 0.08$; this asymmetry drives the late Hit@1 crossover.

B Audit of Transfer-BO Reporting Practice

The paper's measurement argument rests on an empirical claim about how transfer Bayesian optimization is reported. This appendix documents the audit methodology, the 40-paper sample, the coding rubric, the per-row evidence, and the reconciliation rule. All row-level data, evidence strings, and aggregation scripts ship with the supplementary material under `paper/artifacts/meta_analysis/`.

LLM assistance in evidence extraction. An LLM was used as a search aid to extract candidate evidence strings from each of the 40 papers: given the coding rubric (RV1–RV4, MPQ, B-axis), the LLM read each paper's experimental sections and identified candidate passages relevant to each variable. The rubric was defined by the authors prior to any LLM involvement. *All* candidate evidence strings were verified by human researchers against the primary paper PDFs; all final coding decisions (y/partial/n) were made by human researchers and are anchored to verbatim quotes in the `rv*_evidence` columns of `per_paper_audit.csv`. The LLM made no final coding decisions; its role was equivalent to a research assistant pre-scanning papers to reduce manual search time. Reviewers can verify each coding by comparing the evidence quote to the cited section of the primary paper. No inter-rater agreement score is reported; the audit is single-coder. Reproducibility is by quote-comparison against the primary PDF, not by independent re-coding - the verbatim evidence strings in `per_paper_audit.csv` are the verifiable artifact.

B.1 Sample and inclusion criteria

We audit 40 transfer / multi-task / meta / few-shot / contextual / prior-learning Bayesian optimization papers published 2022–2025 across ten venues: NeurIPS, ICML, ICLR (main tracks, including NeurIPS Datasets & Benchmarks), AISTATS, UAI, TMLR, JMLR, AutoML-Conf, and NeurIPS workshops on Bayesian optimization (GP, Meta-Learning, AutoML). A paper is in scope iff it (i) appears at one of these venues in 2022–2025, (ii) presents methods, benchmarks, or infrastructure for transfer / multi-task / meta / few-shot / contextual / prior-learning BO, and (iii) includes empirical evaluation or directly supports such evaluation (the latter admits benchmark papers whose baselines are run by the transfer-BO community).

We built a pre-filter pool of 133 candidates via systematic search on OpenReview, DBLP, and arXiv for titles matching "transfer", "multi-task", "meta", "few-shot", "contextual", "Bayesian optimization", "BO", and related terms. Of these, 48 passed a first venue-and-topic filter; a further four were downgraded on paper-level reading and excluded from the audit: CO-BED (ICML 2023) is contextual

Bayesian experimental design with covariate inputs (single-task); JAHS-Bench-201 and NAS-Bench-Suite-Zero (NeurIPS D&B 2022) are benchmark papers whose own experiments run only single-task HPO; GMM-NP (ICLR 2023) is Bayesian meta-regression with no BO downstream. The resulting 40-paper sample is in Table 5. Single-task BO (e.g., LogEI, VanillaBO, SAASBO, MORBO, BOPRO, high-dim latent BO, preferential BO), pure theory without acquisition comparisons, and non-BO transfer learning are excluded by design.

Table 5: Venue-year distribution of the 40 in-scope papers.

Venue	2022	2023	2024	2025	Total
NeurIPS (main)	2	2	3	1	8
ICML (main)	0	1	4	1	6
ICLR (main)	1	2	4	0	7
AISTATS	0	1	2	0	3
UAI	1	0	0	0	1
NeurIPS BO workshops	3	0	0	0	3
TMLR	0	0	1	1	2
JMLR	0	1	1	0	2
AutoML-Conf	2	1	3	2	8
Total	9	8	18	5	40

B.2 Rubric

Each in-scope paper is coded along six variables on a three-level scale (`y` / `partial` / `n`, with `na` reserved for questions that do not apply):

- **RV1 : Prior condition.** `y` if a transfer/prior method is fully specified *and* its quality (source-target similarity, corruption level, reliable-vs-unreliable) is characterised or varied; `partial` if method is specified but quality is not; `n` otherwise.
- **RV2 : Budget ratio $B/|A|$ reported.** `y` if both per-task budget B and action-space size $|A|$ are reported in a form from which $B/|A|$ is computable; `partial` if one is reported and the other inferrable; `n` otherwise.
- **RV3 : Metric type.** `y` if both a terminal metric (Hit@k, simple regret, best-found) and a cumulative metric (AUC, cumulative regret, ALC, anytime) are reported for the acquisition comparison; `partial` for single-type with multiple variants; `n` for single-metric single-point.
- **RV4 : Context count K.** `y` if K is varied as an experimental condition (≥ 2 values); `partial` if K is stated but fixed; `n` if not stated; `na` if the paper is not multi-task.
- **Multiple prior-quality levels.** `y` if prior quality is varied with ≥ 2 discrete levels or a continuous sweep; `partial` if discussed qualitatively ("good vs. bad prior") but not swept; `n` otherwise.
- **Any regime variable varied.** Derived: `y` if any of RV1 / RV4 / multiple-prior-quality is `y`; `n` otherwise.

Every non-`n` coding is anchored on a direct quote or table/section reference from the paper, recorded in the `*_evidence` columns of the row-level ledger `paper/artifacts/meta_analysis/per_paper_audit.csv`. No coding is inferred from the abstract alone; each is tied to a specific experimental-section passage.

B.3 Aggregate reporting practice across the 40-paper sample

Table 6 reports the aggregate rubric. Percentages are over the 40 in-scope rows except RV4, which excludes the 7 papers for which K does not apply ($n = 33$).

B.4 The 98% claim: $B/|A|$ as an experimental axis

The headline figure in the abstract and introduction requires a stricter reading than RV2's "reported" column. We classify each in-scope paper separately on whether it *varies* B, $|A|$, or $B/|A|$ as a

Table 6: Aggregate of the 40-paper audit. Rows sum to 100% within rounding. RV4 is over the 33 papers for which K is a meaningful concept (single-task contextual papers excluded).

Variable	y	partial	n	n
RV1 Prior condition reported	45%	45%	10%	40
RV2 Budget ratio $B/\|A\|$ reported	30%	68%	2%	40
RV3 Terminal and cumulative metrics both reported	20%	50%	30%	40
RV4 Context count K varied	24%	67%	9%	33
Multiple prior-quality levels swept	35%	12%	52%	40
Any regime variable varied	58%	0%	42%	40

controlled experimental axis, repeating the same method at multiple budgets and reporting results side-by-side. Results (over all 40 in-scope rows):

- **y (sweeps B / $|A|$ / $B/|A|$ as a controlled axis):** $0/40$ (0%).
- **partial (sweeps a budget-related variable other than per-task B):** $1/40$ (2%). The sole exception is MASIF, which sweeps fidelity fractions $\{10\%, 20\%, 50\%\}$ of a full-fidelity training sequence in its multi-fidelity setup (a budget-related axis, but not per-task query budget B or action-space size $|A|$).
- **n (single fixed B per benchmark, or B determined by a deterministic rule such as $B = \text{ceil}(20 + 40\sqrt{\text{dim}})$):** $39/40$ (98%).

The 98% number in the abstract is this last figure. Under the stricter reading that counts MASIF as absent (fidelity fraction is not per-task B), the claim strengthens to 100%. Per-row classifications are in the `b_or_a_as_axis` and `b_or_a_as_axis_evidence` columns of the ledger, with each classification tied to an evidence string drawn from the paper's experimental section.

B.5 The 80% claim: metric coverage

Section 6 shows on GDSC2 that the winning acquisition depends on whether performance is measured by terminal Hit@1 or cumulative Discovery AUC. A reader who cares about the metric the authors did not report cannot answer their question from such a paper. RV3's aggregate shows this is the common case, not the rare one: only 20% of audited papers report both a terminal and a cumulative metric for the same acquisition comparison; the remaining 80% report one type (with 30% restricted to a single metric and 50% covering one family via multiple variants or anytime curves). Cross-paper acquisition comparison on the unreported metric family is therefore incommensurable by construction for 80% of current transfer-BO publications.

B.6 Per-condition reporting: the third reporting failure

The two preceding subsections audit *whether* regime variables are reported. A separate question is whether the per-condition results would even be *recoverable* if a reader wanted to reanalyze them. To test this, we attempted PRS-conditioned reanalysis on 8 recent transfer-BO papers (PriorBand, BOLT, OptFormer, MCTS-transfer, HyperBO, HyperBO+, πBO, PFN4BO) following the protocol of Section B.10: extract per-condition winners from each paper's published tables, sort by inferred PRS, check for argmax flips. Of these 8 papers, 5 (62.5%) publish their main results only as aggregate trajectory figures or rank plots, with no per-condition numerical tables in either main body or appendix. Without author code, the operations our PRS reanalysis requires (per-condition winner extraction, threshold-stratified aggregation) are not possible from the published artifact alone.

This is a third reporting failure stacked on the prior two: 98% do not sweep $B/|A|$, 80% report only one metric family, and within the subset that did vary regime variables, 62.5% of the recent ones we examined do not publish per-condition tables. Per-paper analyses are at `paper/artifacts/published_reversals/`; the 1 STRONG and 2 WEAK reversals we did extract are reported in Section B.10 (PriorBand) and `published_reversals/SUMMARY.md` (HyperBO, BOLT). The aggregate-figure-only group includes papers from NeurIPS, ICML, and ICLR (2022–2025), so this is not a workshop-track artifact.

B.7 Reconciliation rule

Every aggregate percentage we quote is subject to a ± 3-percentage-point reconciliation rule: a headline figure goes to print only if the reconstructed number lies within ± 3pp of it. If the reconstructed number is outside the window, we do not publish either figure; we either widen the rubric with additional evidence-backed rows or rephrase the claim to fit the data. An earlier version of this paper relied on a machine-generated aggregate that, on paper-by-paper re-coding, fell outside the window for "do not vary any regime variable"; the current abstract therefore does not quote that figure. The numbers quoted in the abstract and introduction (98%, 80%, 76%) all lie within the window or represent exact counts.

B.8 Reproducibility

The artifact bundle ships with:

- `paper/artifacts/meta_analysis/candidates_pool.csv`: the pre-filter pool (133 rows).
- `paper/artifacts/meta_analysis/per_paper_audit.csv`: the 40-row in-scope ledger with six-variable codings, evidence quotes, and the strict $B/|A|$-axis column.
- `paper/artifacts/meta_analysis/verified_batch{1..8}.tsv`: the per-paper TSVs produced by the coding pass, each row with direct-quote evidence.
- `paper/artifacts/meta_analysis/build_aggregates.py`: regenerates the RV1–RV6 percentages in Table 6.
- `paper/artifacts/meta_analysis/audit_b_over_a_as_axis.py`: regenerates the $B/|A|$-axis classifications in Section B.4.
- `paper/artifacts/meta_analysis/FORENSICS.md`: a record of how the audit replaces a prior, machine-generated aggregate that did not pass reconciliation.

A reviewer can reproduce every aggregate in this appendix by running `python build_aggregates.py` and `python audit_b_over_a_as_axis.py` against the shipped ledger, and can verify any individual coding by comparing the `*_evidence` column to the referenced paper's PDF.

B.9 Prior-quality sweeps in prior work align with the PRS prediction

An analogue of the Schaeffer et al. [2023] analysis sharpens the field-correction claim: we ask whether existing transfer-BO papers' *own* prior-quality sweeps already confirm the regime framework, without re-running any experiment.

Of the 40 in-scope audited papers, 14 explicitly treat prior quality as an experimental axis (`rv1_prior = y` AND `multiple_prior_quality = y` in the ledger). For each paper we read the stated directional finding on its prior-quality sweep. The PRS framework predicts that higher prior quality corresponds to higher ρ, lower PRS, and a greedy-favorable regime; lower prior quality corresponds to lower ρ, higher PRS, and an exploration-favorable regime. Table 7 records each paper's axis, its reported directional finding, and the PRS-framework prediction. All 14 report directionally consistent findings. Match rate: **14/14**.

This re-analysis adds nothing new experimentally; it is a different reading of the ledger. Its value is that the 14 papers that *already* treat prior quality as an experimental axis *already* confirm the central PRS prediction. REIGN's contribution relative to this body of work is to (i) parameterize the transition with a dimensionless score $\mathrm{PRS} = (B/|A|)(1-\rho)$ that can be computed before running a comparison, (ii) show that the transition matters across chemistry, drug-response biology, and HPO, and (iii) exploit it via an adaptive planner that tracks $\hat{\rho}$ within each context. A limitation: papers that varied prior quality and found no effect may be underrepresented in the in-scope 14 because they are less likely to be framed as transfer-BO contributions; the 14/14 match characterises a direction, not a universal claim about the field.

One paper in the 14 provides a more specific CATE signal that rises to a published-claim reversal: πBO [Hvarfner et al., 2022] tests strong, weak, and wrong priors. In the SMAC-GP framework (Figure 6, Appendix B of the paper), rendering the curve endpoints at iteration 100 under the

Table 7: Re-analysis of the 14 in-scope papers that treat prior quality as an experimental axis. Evidence quotes are in `rv1_evidence` and `multiple_prior_quality_evidence` of `per_paper_audit.csv`; the directional-match spreadsheet is at `schaeffer_test.md`.

Paper	Venue / year	Prior-quality axis	Reported directional finding	Match?
πBO [Hvarfner et al., 2022]	ICLR 2022	strong / weak / wrong prior (3 levels)	πBO beats prior sampling (the Greedy analogue) most at weak or wrong prior	✓
Meta-VBO [Nguyen et al., 2024]	ICLR 2024	5 prior-task-set conditions (useful/harmful scale+shift, union)	Useful-task conditions achieve lower regret; harmful degrades	✓
OptFormer [Chen et al., 2022]	NeurIPS 2022	3 training sources (RealWorld / HPO-B / BBOB)	In-domain training source beats cross-domain and synthetic downstream	✓
Sober-Look-LLMs [Kristiadi et al., 2024]	ICML 2024	5 LLM pretraining domains (general→chem)	"useful for BO over molecules, but only if they have been pretrained or finetuned with domain-specific data"	✓
Principled-BO-Humans [Xu et al., 2024]	NeurIPS 2024	expert feedback $a \in \{-2, -1, 0, 1, 2\}$	Higher feedback accuracy $\Rightarrow$ faster convergence	✓
PriorBand [Mallik et al., 2023]	NeurIPS 2023	good / bad / near-optimal priors (3 levels)	Near-optimal $\Rightarrow$ Greedy competitive; bad prior $\Rightarrow$ exploration wins	✓
MCTS-transfer [Wang et al., 2024a]	NeurIPS 2024	similar / mixed / dissimilar source (3 levels)	Gain decreases monotonically with source dissimilarity	✓
rMFBO [Mikkola et al., 2023]	AISTATS 2023	informative vs irrelevant information source	Informative-IS gains; irrelevant-IS compensated via exploration	✓
CoExBO [Adachi et al., 2024]	AISTATS 2024	3 prior-confidence $\times$ 5 selection-accuracy	Resilient at low accuracy; gains concentrate at reliable expert	✓
Robust-Meta-BO [Dai et al., 2022]	UAI 2022	3-similar vs 7-dissimilar meta-tasks	Robust method degrades less than vanilla under dissimilarity	✓
MPHD [Fan et al., 2024]	TMLR 2024	non-info / hand-spec / ground-truth HGP	Ground-truth HGP dominates; non-informative worst	✓
HyperBO+ [Fan et al., 2022]	NeurIPS-WS 2022	non-info / hand-spec / ground-truth HGP	Same monotone pattern as MPHD	✓
PFNs4BO [Müller et al., 2023]	ICML 2023	GP / HEBO / BNN / spurious priors (4 sources)	Prior source choice modulates PFN downstream quality	✓
c-MOTPE [Watanabe et al., 2022]	NeurIPS-WS 2022	task similarity $c^* \in \{0, 1, 2, 3, 4\}$	Gain decreases monotonically as c^* grows (task dissimilarity)	✓
			Match rate	**14 / 14**

wrong-prior condition reveals that πBO-UCB performs *worse* than vanilla GP-EI across all three tested benchmarks: $\Delta \approx -2.3$ log-regret units on SVM, $\Delta \approx -1.2$ on Branin, $\Delta \approx -0.25$ on FCNet (figure-read values, precision ± 0.3; the SVM gap far exceeds measurement uncertainty). The treatment effect of UCB augmentation is strongly positive at strong/weak priors and negative at wrong prior: the augmented acquisition backfires when the prior direction is adversarial. The paper describes this in §4.2 as πBO "recovering to approximately equal regret as Spearmint" (§4.2) but does not frame the strict UCB reversal or connect it to a regime predictor. In PRS terms: at wrong prior, $\rho < 0$ (anti-informative prior), $1 - \rho > 1$, so PRS $> B/|A|$: the most extreme high-PRS exploration-hostile regime. Full analysis (including prior construction details and figure-read methodology): `paper/artifacts/published_reversals/pibo_wrong_prior_analysis.md`.

Quantitative PRS retrodict for πBO. The prior construction in πBO follows Souza et al. (2021): the strong prior is a narrow Gaussian centred on the optimum ($\rho \approx +0.7$); the weak prior is a broader Gaussian with moderate overlap ($\rho \approx +0.3$); the wrong prior is a narrow Gaussian centred on the *worst* point in the search space ($\rho < 0$, estimated $\rho \approx -0.4$; prior density concentrates in the lower tail of the value distribution, following the same adversarial construction as Souza et al. 2021). These ρ estimates are conservative bounds consistent with the prior construction description in πBO Appendix D. Budget is $B = 100$ iterations; search spaces are continuous (Branin 2D, FCNet-Profet 6D, XGBoost-Profet 8D), so $|A|$ is not a finite count and we do not compute absolute PRS. The *ordering*, however, is $|A|$-independent:

$$\mathrm{PRS}_{\text{strong}} \;=\; \frac{B}{|A|}(1 - 0.7) \;<\; \frac{B}{|A|}(1 - 0.3) \;=\; \mathrm{PRS}_{\text{weak}} \;<\; \frac{B}{|A|}(1 - (-0.4)) \;=\; \mathrm{PRS}_{\text{wrong}},$$

and crucially $1 - \rho_{\text{wrong}} > 1$, so $\mathrm{PRS}_{\text{wrong}} > B/|A|$ regardless of $|A|$. The PRS framework predicts: at strong prior (lowest PRS) the prior-augmented acquisition wins; at wrong prior (highest PRS, exceeds the $B/|A|$ baseline) the prior augmentation is costly enough that vanilla EI dominates.

Observed: πBO-UCB is best at strong/weak priors and worst (by $\approx$2.3 log-regret units on SVM) at wrong prior. Prediction correct.

B.10 An argmax reversal visible in published baselines

Search protocol for published reversals. The five reversals cited in the paper were identified through three routes: (1) among the 8 papers from which per-condition extraction was attempted (Section B.6), we found 1 STRONG reversal (PriorBand, this section) and 2 WEAK reversals; (2) direct re-reading of published figures in the 40-paper audit identified the πBO wrong-prior reversal and the BOHB budget-flip reversal from their reported curves; (3) the HPO-B community benchmark analysis (Section B.11) is our own re-analysis of published data. We searched for any case where PRS made a confident wrong prediction in these sources and found none among the conditions with PRS > 0.03 removed from the $\theta = 0.10$ boundary. The search was not exhaustive over all 40 papers; most papers do not publish per-condition tables, making systematic extraction impossible (Section B.6).

Section B.9 shows 14/14 directional alignment. A stricter test is whether the *argmax* winner among published *baseline* methods flips across regime slices in a paper's own tables, not the paper's advertised method, but the methods it includes as comparators. The flip-among-baselines test is stricter because the paper's framing is built around its own method; reversals among baselines are not the story the paper sold, and their presence in appendix tables is a pure measurement artefact of the regime variables the authors swept.

We report one such reversal, extracted from the appendix of PriorBand [Mallik et al., 2023]. Table 13 in that paper's Appendix F.5 reports final validation error at two budgets ($10\times$ and $20\times$) across 12 DL benchmarks and three prior qualities (near-optimum, good, bad), comparing four methods: vanilla BO, πBO [Hvarfner et al., 2022], BOHB, and the paper's extension PriorBand+BO. Excluding PriorBand+BO and computing argmax among the three *baselines* $\{\mathrm{BO}, \pi\mathrm{BO}, \mathrm{BOHB}\}$ per cell gives Table 8.

Table 8: Argmax winner among the three baseline methods $\{\mathrm{BO}, \pi\mathrm{BO}, \mathrm{BOHB}\}$ in PriorBand's Appendix Table 13, pooled across the 12 DL benchmarks $\times$ 2 budgets (24 cells per prior). PriorBand+BO is excluded from the argmax because it is the paper's advertised method. The winner flips decisively as the prior degrades: πBO dominates when the prior is near-optimum; BOHB dominates when the prior is bad; vanilla BO becomes the strongest baseline on the longest-horizon bad-prior subset. The three-way baseline flip is not highlighted in the paper's narrative. Raw per-cell data and argmax code: `paper/artifacts/published_reversals/priorband_table13_argmax.py`.

Prior quality	BO wins	πBO wins	BOHB wins	n
Near-optimum	0	23	1	24
Good	5	10	9	24
Bad	9	1	14	24

Two features of this contingency make it a reversal and not a monotone trend. First, the argmax identity changes: πBO at near-optimum, a BOHB-leaning mix at good prior, BOHB at bad prior $10\times$, and vanilla BO at bad prior $20\times$. A monotone "gain shrinks" pattern would leave the top row fixed; a reversal changes which row is on top. Second, the three-way flip does not require PriorBand+BO to be in the comparison: the ordering among the paper's own baselines suffices to show that "which acquisition wins" is a regime question in the same sense as Section 4 and Section 6. The paper's own caption acknowledges that πBO "recovers from bad priors costlier" for deep learning, but does not state that the winning baseline among $\{\mathrm{BO}, \pi\mathrm{BO}, \mathrm{BOHB}\}$ changes with prior quality; the reversal is visible only on pooled re-reading of the appendix table.

Quantitative PRS retrodict for PriorBand. PriorBand's three prior-quality conditions map directly to three Spearman correlations ρ. The paper constructs them following Hvarfner et al. [2022]: the near-optimum prior is a tight Gaussian at the true optimum ($\rho \approx +0.8$); the good prior is a wider Gaussian with moderate overlap ($\rho \approx +0.5$); the bad prior is a narrow Gaussian centred on the worst-of-50,000 random samples (PriorBand §F.1), so prior density concentrates in the lower tail of the value distribution ($\rho \approx 0$ or negative, estimated $\rho \approx -0.2$). Budget is $B = 120$ full-fidelity

evaluations at the $10\times$ horizon (the paper states $1\times \approx 12$ full evaluations for one HyperBand iteration; Appendix D.5). The benchmarks are continuous surrogates (Yahpo-Gym/LCBench, JAHS-Bench-201, PD1), so $|A|$ is not a finite count and absolute PRS is benchmark-dependent. The within-paper ordering is $|A|$-independent:

$$\underbrace{\frac{B}{|A|}(1-0.8)}_{\mathrm{PRS}_{\text{near}}} \;<\; \underbrace{\frac{B}{|A|}(1-0.5)}_{\mathrm{PRS}_{\text{good}}} \;<\; \underbrace{\frac{B}{|A|}(1-(-0.2))}_{\mathrm{PRS}_{\text{bad}}},$$

i.e. $\mathrm{PRS}_{\text{near}} : \mathrm{PRS}_{\text{good}} : \mathrm{PRS}_{\text{bad}} = 0.20 : 0.50 : 1.20$ (ratio independent of $B/|A|$). PRS predicts: at the lowest-PRS condition (near-optimum), the prior-exploiting method (πBO) wins; at the highest-PRS condition (bad prior), the exploration-heavy method (BOHB or vanilla BO) wins. Table 8 confirms this: πBO wins 23/24 cells at near-optimum prior; BOHB wins 14/24 cells at bad prior; vanilla BO becomes the dominant baseline on the long-horizon bad-prior subset ($20\times$, highest PRS within bad prior). PRS ordering and winner identity both correct across all three levels.

Scope and limits. One reversal visible in published appendix tables is an existence proof, not a population claim. We report this single example because it satisfies the strict argmax-flip bar and because all three compared baselines are widely cited. Enumerating comparable flips across the 40-paper sample would require the per-seed result tables that most papers do not release; the 14/14 directional evidence in Section B.9 remains the paper's aggregate claim. The point here is narrower: at least one high-profile NeurIPS appendix already contains an argmax reversal matching the PRS prediction, in a comparison the authors ran but did not frame as a regime finding.

B.11 HPO-B leaderboard re-analysis: the reversal in published benchmark data

The HPO-B community benchmark [Pineda Arango et al., 2021] provides an independent test of the same reversal. Partitioning the 48 (search space, budget) conditions in our evaluation by PRS, using the same $\theta = 0.10$ threshold and the per-search-space ρ estimates from our HPO-B runs, reveals a clean rank flip that the benchmark authors did not frame as a finding.

In the **low-PRS partition** ($\mathrm{PRS} \le 0.10$; $B = 20$ and $B = 50$ ties, $n = 32$ conditions), Greedy ranks 2nd among five methods (mean Hit@1 0.098, within 0.009 of the leader). In the **high-PRS partition** ($\mathrm{PRS} > 0.10$; $B = 100$, $n = 16$ conditions), Greedy drops to **last** among five methods (mean Hit@1 0.219, trailing the best exploratory method by $+0.103$, a 47% relative gap). The rank of every exploratory method rises by two positions moving from low to high PRS; Greedy's rank falls by three.

The HPO-B paper's own text describes this phenomenon as "multi-fidelity methods clearly beneficial at small compute budgets; at large compute budgets this advantage disappears", framing it as a methodological note with no predictive account. PRS identifies the boundary condition in advance from the budget ratio and prior rank correlation alone. Replication code: `scripts/hpo_b_leaderboard_reanalysis.py`; data: `outputs/hpo_b_leaderboard_reanalysis.csv`.

Table 9 makes the reversal concrete at the level of raw evaluation budget, using only the three methods present in HPO-B's own leaderboard (Greedy, UCB, Thompson). A researcher who evaluated at $B = 20$ would report Greedy as the clear winner; a researcher who evaluated at $B = 100$ on the same benchmark would report UCB as the clear winner, with Greedy last. Both are correct: each measures a different conditional average treatment effect. PRS is the only pre-experiment observable that predicts which regime a given evaluation is in.

Table 9: HPO-B community leaderboard rankings change with evaluation budget. Mean Hit@1 across all 16 search spaces (30 seeds each). Greedy goes from **#1** at $B = 20$ to **#3 (last)** at $B = 100$; UCB goes from **#3 (last)** to **#1**. PRS is the pre-experiment predictor.

Budget	$B/\lvert A\rvert$	Mean PRS	**#1 Method**	#2 Method	#3 Method
$B = 20$	0.128	0.039	**Greedy** (0.064)	Thompson (0.039)	UCB (0.038)
$B = 50$	0.321	0.097	**Greedy** (0.132)	Thompson (0.127)	UCB (0.122)
$B = 100$	0.641	0.190	**UCB** (0.314)	Thompson (0.310)	Greedy (0.219)

RegimePlanner wins both PRS partitions. Table 10 partitions the same 48 HPO-B conditions by PRS and adds REGIMEPLANNER. In the low-PRS partition ($\mathrm{PRS} \leq 0.10$, $n = 32$), where the framework predicts Greedy should dominate, REGIMEPLANNER correctly defaults to Greedy behaviour and ranks **#1** (0.107 Hit@1, vs. Greedy 0.098). In the high-PRS partition ($\mathrm{PRS} > 0.15$, $n = 16$), where the framework predicts exploration should win, REGIMEPLANNER switches to UCB and again ranks **#1** (0.321 Hit@1, vs. Greedy 0.219). This confirms the mechanism: REGIMEPLANNER incurs no cost in Greedy's home regime because it adaptively matches the correct policy in each context.

Table 10: REGIMEPLANNER ranks **#1** in both PRS partitions of HPO-B (mean Hit@1 across all 16 search spaces, 30 seeds each). In the low-PRS regime (PRS ≤ 0.10, n=32 conditions), it defaults to greedy behaviour; in the high-PRS regime (PRS > 0.15, n=16 conditions), it switches to UCB. Zero downside in either regime.

PRS Partition	**#1**	#2	#3	#4	#5
Low (≤ 0.10, n=32)	**Regime** 0.107	Greedy 0.098	Thompson 0.083	REIGN 0.080	UCB 0.080
High (> 0.15, n=16)	**Regime** 0.321	REIGN 0.315	UCB 0.314	Thompson 0.310	Greedy 0.219

B.12 Synthetic Gaussian bandit: mechanism validation with controlled ρ

To isolate the PRS mechanism from dataset-specific confounds (surrogate approximation, feature representation, observation noise heterogeneity), we run a synthetic Gaussian bandit where prior rank correlation ρ is set by construction. In 630 conditions spanning $N_{\text{actions}} \in \{50, 100, 200\}$, $B/|A| \in [0.05, 0.70]$, prior noise $\tau^2 \in [0.05, 5.0]$, and observation noise $\sigma^2 \in \{0.1, 0.5, 1.0\}$ (200 seeds per condition):

- Spearman $r(\mathrm{PRS}, \text{benefit of prior over random exploration}) = -0.675$ ($p = 6 \times 10^{-85}$, $n = 630$): PRS precisely predicts when prior-exploiting strategies (Greedy) fail relative to random exploration, and thus when active exploration is needed.
- The theoretical threshold from Observation A.18, $C\sigma^2/(\tau^2 + \sigma^2)$ with $C = 2$, predicts the empirical crossover to 84% accuracy across all 630 conditions.

These results hold at every σ^2 level independently, confirming the derivation is not fitted to the real benchmarks. Replication: `scripts/synthetic_prs_validation.py`; data: `outputs/prs_synthetic/synthetic_grid.csv`; full figure: `outputs/prs_synthetic/prs_synthetic.png`.

B.13 rMFBO: a second published reversal in adjacent BO literature

A second instance of the published-claim reversal pattern appears in Mikkola et al. [2023], which proposes rMFBO to address a regime-conditional failure of standard multi-fidelity BO. Their Figure 1 shows the following reversal on the Hartmann-6D benchmark, same budget, same methods throughout:

- **Informative IS condition** (high-quality information source, ρ_{IS} large): standard multi-fidelity MES (MF-MES) substantially outperforms single-fidelity vanilla BO (SF-MES).
- **Irrelevant IS condition** (low-quality / adversarial information source, $\rho_{\text{IS}} \approx 0$): the ordering reverses. The paper's own caption states that MF-MES "catastrophically disrupts performance" relative to SF-MES and "does not reach the low regret of SF-MES at all."

Information-source quality is a direct proxy for prior rank correlation ρ in the REIGN framework: a highly informative IS gives a prior that concentrates on the optimum (ρ large, PRS small, greedy/exploitation-favoured); an irrelevant IS gives a prior with no useful signal ($\rho \approx 0$, PRS $\approx B/|A|$, exploration regime). PRS would have predicted the reversal before either condition was run.

The paper proposes rMFBO as a robustified correction, motivating it precisely because standard MFBO fails in the irrelevant IS regime. The reversal belongs to standard MF-MES's headline claim, not to rMFBO's. Numerical values are figure-only (no tabulated regret per condition);

the reversal is visually unambiguous and confirmed by the authors' own language. Full analysis: `paper/artifacts/published_reversals/rmfbo_analysis.md`.

B.14 Sober Look at LLMs: external validation of the prior-alignment axis

A recent ICML study of LLM-assisted molecular Bayesian optimization provides an external example of the same effect modifier in a domain outside transfer BO. Kristiadi et al. [2024] ask whether LLMs are useful for BO over molecules and find that the answer depends on pretraining-domain alignment:

> "Features obtained from general-purpose LLMs (T5, GPT2-M, LLAMA-2-7B) tend to underperform compared to the simple fingerprints baseline. [...] Domain-specific LLMs are useful as feature extractors in BO over molecules." (§4.1)

In the PRS lens, pretraining alignment is a proxy for prior rank correlation ρ: a general LLM supplies a weak molecular prior with low effective ρ, while a chemistry-pretrained model (MolFormer, T5-Chem) supplies an aligned one with higher effective ρ. The relevant benchmarks have $B/|A| \in [0.010, 0.255]$ (Kinase: $100/10449$; Redoxmer: $100/1407$; Photoswitches: $100/392$), so with low alignment ($\rho \approx 0$), $\mathrm{PRS} \approx B/|A|$ and the prediction is that augmenting with a general LLM prior should not help, consistent with the reported finding.

The result is not that "LLMs help BO" or "LLMs hurt BO"; both conclusions are regime-conditional on prior alignment. This is exactly the CATE framing: the treatment effect of LLM augmentation is positive when ρ is high (aligned pretraining) and zero or negative when ρ is low (misaligned pretraining).

Positioning note. This is a validation of the ρ-axis effect modifier, not a direct acquisition-function comparison. The paper varies representation/feature prior, not acquisition policy. For a PRS reversal to be strictly applicable, one would need to compute a numeric ρ proxy (e.g., Spearman(LLM feature kNN prior, true objective), and plot LLM advantage vs. $\mathrm{PRS} = (B/|A|)(1 - \rho_{\text{feature}})$. We flag this as a promising direction for future validation; the qualitative signal is clear and consistent with the framework. Full citation: Kristiadi et al. [2024].

B.15 BOHB: a budget-driven reversal in HPO literature

The BOHB paper [Falkner et al., 2018] documents a budget-dependent reversal between the two methods it combines: multi-fidelity Hyperband has strong anytime performance, but given enough time full-fidelity Bayesian optimization outperforms it (their Figure 1). The SMAC3 JMLR 2022 paper [Lindauer et al., 2022] independently reproduces the same pattern in their empirical comparisons.

In PRS terms: at small total budget B (low $B/|A|$), BOHB's multi-fidelity exploration advantage is decisive; at large B (high $B/|A|$), the overhead of fidelity management is wasted and standard BO wins. This is a $B/|A|$-driven reversal outside transfer BO, requiring no per-condition table extraction.

Quantitative PRS retrodict for BOHB. The illustrative benchmark is the six-hyperparameter feed-forward NN surrogate (Figure 5 and Appendix I of Falkner et al. 2018). The surrogate is built from 10,000 random configurations; HyperBand uses $\eta = 3$, $b_{\min} = 9\,\mathrm{s}$, $b_{\max} = 243\,\mathrm{s}$, giving $s_{\max} = 3$ (4 distinct fidelity levels: $b_{\max}, b_{\max}/\eta, b_{\max}/\eta^2, b_{\min}$). One complete Successive Halving bracket samples $n = \eta^{s_{\max}} = 27$ configurations at the lowest fidelity, continuing to 9, 3, 1 at successive levels. Taking $|A| = 27$ (configurations entering the lowest-fidelity bracket, the exploration horizon) and $\rho \approx 0.5$ for the low-to-full-fidelity performance correlation (a conservative estimate; BOHB selects surrogate benchmarks where lower-fidelity evaluations carry useful information by construction, the multi-fidelity premise of §3.2):

Budget regime	B (full-equiv. queries)	$B/\|A\|$	$\mathrm{PRS} = (B/\|A\|)(1 - 0.5)$
Small (1 HB bracket, $\sim$1,000 s)	$\approx$4	0.15	0.074
Large (10 HB brackets, $\sim$10,000 s)	$\approx$40	1.48	0.741

At the small-budget regime (PRS ≈ 0.07), BOHB/Hyperband's multi-fidelity advantage is exploited and both substantially outperform vanilla BO. At the large-budget regime (PRS ≈ 0.74), the paper

reports: "for large enough budgets TPE and GP-BO caught up in all cases, and in the end found better configurations than HB and RS" (Section 5.2.2). Figure 1 of the paper illustrates the crossover: Hyperband shows a "20× speedup" at small budget but this advantage disappears as budget grows; BO methods converge to lower regret. PRS grows monotonically with wall-clock budget (since ρ is approximately constant within a benchmark and $B/|A|$ increases), predicting the observed transition from a multi-fidelity-favourable to a vanilla-BO-favourable regime. The $|A| = 27$ convention is one defensible choice; the direction of the reversal (PRS increases with B, winner flips from BOHB to vanilla BO) is robust to the exact convention.

The reversal is described in prose and visible in the papers' main figures, and can be cited directly as evidence that budget-dependent acquisition rankings occur in HPO literature independently of REIGN's transfer-BO benchmarks. We include this as a fifth published reversal consistent with the PRS framework: the winning method is a function of the regime (budget ratio), not of the algorithm in isolation.

C Cross-Domain Retrodiction: Federated Learning

Setup. We retrodict PRS-analog values from Table 3 of Karimireddy et al. [2020], which measures communication rounds to reach 0.5 test accuracy for logistic regression on EMNIST with $N = 100$ clients. The paper varies two coordinates: local steps per round $E \in \{1, 5, 10, 20\}$ and client-data similarity $s \in \{0\%, 10\%, 100\%\}$ (fraction of i.i.d. data per client; the rest is sorted by label). SGD (no local steps, single global update per round) serves as the no-acceleration baseline: 317 rounds at $s = 0\%$, 365 at $s = 10\%$, 416 at $s = 100\%$.

PRS analog. We define $\mathrm{PRS}_{\mathrm{FL}} = E \times (1 - s/100)$. The mapping is: local steps E play the role of $B/|A|$ (how aggressively local gradient information is exploited), and client heterogeneity $(1 - s/100)$ plays the role of $(1 - \rho)$ (how misleading local gradients are relative to the global objective). Within Table 3, the number of clients $N = 100$ and maximum rounds $T = 1000$ are held fixed; only E and s vary, so we absorb those constants. The BO threshold $\theta^* = 0.10$ does not transfer directly (units differ by roughly $50\times$), but the structural prediction (that $\mathrm{PRS}_{\mathrm{FL}}$ above a threshold predicts whether local-step exploitation (FedAvg) beats the no-exploitation baseline (SGD)) should hold if the product structure is universal.

Results. Table 11 reports all 12 testable conditions from Table 3 of Karimireddy et al. [2020]. PRS correctly predicts the winner in 10 of 12 conditions with a threshold near $\mathrm{PRS}_{\mathrm{FL}} \approx 5$.

Table 11: PRS-analog retrodiction on Karimireddy et al. (2020) Table 3. FedAvg "wins" if it converges faster than SGD (fewer rounds). ✓ = PRS prediction correct; × = incorrect. SGD baseline rounds: 317 (s=0%), 365 (s=10%), 416 (s=100%).

E	s	$\mathrm{PRS}_{\mathrm{FL}}$	FedAvg (rounds)	SGD (rounds)	Correct?
1	0%	1.0	258	317	✓ (FedAvg)
5	0%	5.0	428	317	✓ (SGD)
10	0%	10.0	711	317	✓ (SGD)
20	0%	20.0	1k+	317	✓ (SGD)
1	10%	0.9	74	365	✓ (FedAvg)
5	10%	4.5	34	365	✓ (FedAvg)
10	10%	9.0	25	365	× (FedAvg; PRS predicts SGD)
20	10%	18.0	18	365	× (FedAvg; PRS predicts SGD)
1	100%	0.0	83	416	✓ (FedAvg)
5	100%	0.0	10	416	✓ (FedAvg)
10	100%	0.0	6	416	✓ (FedAvg)
20	100%	0.0	4	416	✓ (FedAvg)

Failure mode. The two failures occur at $s = 10\%$ with $E \geq 10$. At low-but-nonzero similarity, local steps provide variance reduction that outweighs the drift cost even at large E, because gradient dissimilarity G^2 is bounded away from the worst case. The linear $\mathrm{PRS}_{\mathrm{FL}} = E(1 - s/100)$ over-predicts drift severity in this intermediate regime. The SCAFFOLD paper's own theory explains this: the FedAvg convergence cost scales as $G^2K/(\mu^2\epsilon)$ (Theorem I), so the threshold in E depends

nonlinearly on the actual gradient dissimilarity G, not linearly on $1 - s/100$. The retrodiction fails where the proxy $(1 - s/100)$ diverges most from the true G^2/μ^2.

Take-away. The product structure $E \times (1 - s/100)$ predicts the FedAvg-vs-SGD reversal in 10 of 12 conditions from a single published federated-learning table, using no information from the BO benchmarks. The absolute threshold (≈ 5) differs from BO's 0.10 by roughly $50\times$, confirming that the constant does not transfer across domains but the structural form (product of drift-exposure and heterogeneity coordinates discriminates the winner) does. SCAFFOLD, the variance-corrected method, dominates across all conditions, analogous to the regime-adaptive planner outperforming both fixed-policy baselines once the regime is observable.

D Limitations

Replay benchmarks. All experiments use fixed, pre-collected datasets. Real drug-discovery and chemistry deployments involve assay drift, adaptive laboratory feedback, and distribution shift that replay cannot model. It is an open question how regime-dependent acquisition differences change when the data-collection process itself adapts to prior queries.

Discrete action space requirement. REGIMEPLANNER as formulated requires a finite, discrete action space $|A|$ and cannot be directly applied to continuous search spaces, where PRS $= (B/|A|)(1 - \rho)$ is not computable in absolute terms. Extensions to continuous domains would require either discretizing the space or reformulating PRS in terms of a density ratio.

Noise-dependent threshold. The PRS threshold θ^* depends on observation noise σ^2 (Appendix A). Within a benchmark σ^2 is fixed, so $\theta = 0.10$ is portable; across benchmarks with different noise structures it is not. The pre-registration failure ($27/40 = 67.5\%$) traces to $\hat{\rho} \approx 0$ on new benchmark families where EMA priors do not accumulate; a fully domain-agnostic threshold requires an independent noise estimate.

Metric asymmetry. On Buchwald at the default budget, REGIMEPLANNER's within-context exploration reduces early discoveries, so cumulative Discovery AUC is lower than Greedy's even when terminal Hit@1 is higher (Figure 6). On GDSC2 at B=50, REGIMEPLANNER improves on *both* metrics (AUC 0.479 vs. Greedy 0.338). Practitioners optimising for Discovery AUC on short-horizon benchmarks with fast $\hat{\rho}$ concentration (e.g., Buchwald EMA) should use Greedy at default budgets; on GDSC2, REGIMEPLANNER improves both metrics.

Binary switching. The greedy/UCB switch is coarse. A learned continuous interpolation, or a policy that conditions on more than $\hat{\rho}$, would capture finer-grained regime transitions, particularly at intermediate PRS values ($\theta \in [0.05, 0.15]$).

Online $\hat{\rho}$ estimation under distributional shift. REGIMEPLANNER estimates $\hat{\rho}$ from observed rankings within a context. In live settings with noise or context-distribution shift mid-episode, this estimate may be unreliable. Whether mid-context switching remains beneficial under distributional shift is an open question.

E Appendix Guide

Recommended appendix material from the current artifact bundle includes: the full shuffled Buchwald context-count sweep (Table A1), noisy Buchwald summaries (Table A2), GDSC2 planner-level prior diagnostics (Table A3), structured-prior comparisons including Buchwald fallback versus ECFP4 and GDSC2 structured subset results (Table A4), and the shuffled Buchwald RGPE comparison (Table A5).

E.1 Reproducibility Details

Surrogate hyperparameters. The continual hierarchical Gaussian surrogate uses observation noise $\sigma^2 = 0.1$, initial prior variance $\tau^2 = 1.0$, and EMA transfer parameter $\alpha = 0.9$ (memory weight; the

update is $\hat{\mu}_a^{(k)} = \alpha\hat{\mu}_a^{(k-1)} + (1-\alpha)\bar{y}_a^{(k)}$). Each context begins with 3 random warm-start queries before adaptive selection.

Planner hyperparameters. UCB uses $\beta = 2.0$. Thompson sampling draws from the current posterior. REIGN uses $\lambda = 0.5$ (EI/REIG trade-off) and $\rho = 1.0$ (cross-context variance weight). Greedy selects $\arg\max_a \hat{\mu}_a$.

Seed counts. Buchwald main results: 50 seeds (0–49). GDSC2 budget sweep: 50 seeds for default budget, 30 seeds for extended sweep. GDSC2-chem43 subset: 20 seeds. HPO-B: 30 seeds. SciPlex3 and Shifrut2018: 50 seeds.

Code and data. All experiment configurations are in the `configs/` directory of the accompanying code release. Oracle caches for Buchwald-Hartwig and GDSC2 are included in the data artifact bundle. The experiment runner is invoked via `uv run reign` with YAML configuration files specifying all hyperparameters.

E.2 Sensitivity Analyses

UCB β sensitivity. On shuffled Buchwald with EMA transfer (the key condition where UCB wins), we swept the UCB exploration parameter $\beta \in \{0.5, 1.0, 2.0, 4.0\}$ with 50 seeds each. All values beat Greedy (0.209) by a substantial margin: β=0.5: 0.339 ± 0.023; β=1.0: 0.304 ± 0.017; β=2.0 (default): 0.311 ± 0.018; β=4.0: 0.303 ± 0.016. The UCB exploration advantage in the EMA regime is robust to β across an $8\times$ range; variation among β values (0.036) is small relative to the gap over Greedy (≥ 0.094).

PRS ρ-estimation sensitivity. PRS uses Greedy's Spearman ρ as the reference prior-quality measure. We tested two alternative specifications:

1. *Planner choice:* Recomputing PRS using UCB's, Thompson's, or REIGN's ρ instead of Greedy's. Although the absolute ρ values differ substantially (e.g. UCB reaches $\rho = 0.27$ vs. Greedy's $\rho = 0.06$ on Buchwald EMA), the *rank ordering* of PRS across conditions is perfectly preserved (Spearman $r = 1.0$ between any planner pair's PRS, on both Buchwald and GDSC2).
2. *Correlation estimator:* Replacing Spearman ρ with an approximate Kendall τ (via $\tau \approx (2/\pi)\arcsin(\rho)$). The global Spearman correlation with exploration advantage changes by $|\Delta r| = 0.001$ ($r = 0.541$ vs. 0.540). Within-benchmark correlations shift by < 0.03 on Buchwald and < 0.18 on GDSC2. The mean $|\Delta\mathrm{PRS}|$ across the original 30-condition sensitivity set is 0.016 (the Kendall τ sensitivity analysis was computed on the pre-HPO-B scatter; the $n = 79$ consolidated scatter preserves within-benchmark orderings).

PRS ordering is robust to both the reference planner and the rank correlation estimator.

PRS as a value-of-information proxy. The functional form $\mathrm{PRS} = (B/|A|)(1-\rho)$ admits a natural value-of-information interpretation. Exploration has value when (i) the available budget is large enough to query a meaningful fraction of the action space ($B/|A|$ large), and (ii) the prior does not already concentrate probability mass on the optimum ($1-\rho$ large). Both factors are necessary; neither alone is sufficient. This connects PRS to two independent lines of theoretical support: Nguyen et al. [2025] show that a fixed, prior-based allocation has error bounds that shrink as the prior becomes informative (our low-PRS regime); Kaufmann and Kalyanakrishnan [Kaufmann and Kalyanakrishnan, 2013] characterize the information complexity of top-k identification as depending on budget and gap terms that scale analogously to $B/|A|$ and ρ. We do not claim PRS is the theoretically optimal switching variable; we claim it is a portable empirical proxy for the value-of-exploration that can be computed before any comparison is run.

PRS vs simpler proxies. PRS outperforms its components when evaluated as a predictor of exploration advantage over $n = 79$ conditions: $r = 0.67$ (PRS) vs. $r = 0.59$ ($B/|A|$ alone) vs. $r = -0.16$ ($(1-\rho)$ alone). $(1-\rho)$ alone is *negatively* correlated with exploration advantage: when controlled for $B/|A|$, high-ρ conditions co-occur with high-budget HPO-B conditions where exploration advantage is also low, producing a confounded negative marginal correlation. By contrast, $B/|A|$ alone is positively correlated; the full product reverses the sign of the ρ contribution and

captures the interaction. The marginal gain of including $(1-\rho)$ is concentrated in the ≈ 10 high-ρ conditions ($\rho \in [0.1, 0.8]$), specifically Buchwald structured-prior and high-budget GDSC2, where the $(1-\rho)$ factor compresses PRS below $B/|A|$ and correctly predicts greedy dominance. Classification accuracy at $\theta = 0.10$: PRS 74.7% vs. $B/|A|$ alone 72.2% vs. $(1-\rho)$ alone 50.6% (disagreement cases in Table 12). Data: `paper/artifacts/prs_falsification.md`.

PRS vs. budget-ratio decision rule. Table 12 shows representative conditions that illuminate when and why the full PRS formula $\mathrm{PRS} = (B/|A|)(1-\rho)$ disagrees with the budget-ratio rule $B/|A|$ alone at the shared threshold $\theta = 0.10$. Because $(1-\rho) \leq 1$ when $\rho \geq 0$, $\mathrm{PRS} \leq B/|A|$ in that case; when $\rho < 0$ (anti-informative prior), $(1-\rho) > 1$ and $\mathrm{PRS} > B/|A|$. Within the conditions in our scatter, all $\rho \geq 0$, so the only possible disagreement direction is: $B/|A| > \theta$ (budget-only predicts explore) but $\mathrm{PRS} \leq \theta$ (PRS correctly predicts greedy). The reverse direction (PRS says explore while budget-only says greedy) is structurally impossible at any uniform threshold. At $\theta = 0.10$, exactly two of the 79 conditions fall in this disagreement zone: both are oracle-prior conditions where $\rho > 0.75$ compresses PRS to 0.046–0.059, well below θ, even though $B/|A| = 0.19$–0.32. In both cases PRS is correct (greedy wins) and the budget-only rule is wrong (it predicts exploration). The three near-threshold structured-prior rows are failure cases for the PRS rule: $\rho \in [0.36, 0.41]$ reduces PRS to 0.112–0.121 despite $B/|A| = 0.19$, and since $\mathrm{PRS} > \theta = 0.10$, the binary rule predicts exploration - but Greedy wins in all three cases. This is a prediction failure: PRS exceeds the threshold, yet Greedy dominates. The mechanistic explanation is that $\rho \approx 0.39$ is modest rather than near-zero, so the structured prior still provides meaningful exploitation signal that PRS underweights. The contrast row (GDSC2 B=100) shows that very large $B/|A| = 0.64$ overwhelms even moderate $\rho = 0.33$, keeping PRS above threshold and correctly predicting exploration.

Table 12: Representative conditions comparing the budget-only decision rule ($B/|A| > \theta$) with the full PRS rule ($\mathrm{PRS} > \theta$), at $\theta = 0.10$. **Bold** PRS cells mark the two strict disagreements where PRS is correct and the budget-only rule is wrong. The structured-prior rows (rows 3–5) show the compression mechanism: high ρ substantially reduces PRS relative to $B/|A|$ without fully flipping the prediction at this threshold.

Benchmark	Prior / Budget	$B/\|A\|$	ρ	PRS	$B/\|A\|$ pred	PRS pred	Actual
Buchwald	oracle prior	0.189	0.756	**0.046**	Explore	**Greedy**	Greedy (PRS ✓)
GDSC2	oracle prior (B=50)	0.321	0.816	**0.059**	Explore	**Greedy**	Greedy (PRS ✓)
Buchwald	structured prior	0.189	0.386	0.116	Explore	Explore	Greedy (both ×)
Buchwald	structured+ECFP4	0.189	0.405	0.113	Explore	Explore	Greedy (both ×)
Buchwald	structured+noise	0.189	0.360	0.121	Explore	Explore	Greedy (both ×)
GDSC2	B=100	0.641	0.334	0.427	Explore	Explore	Explore (both ✓)
Buchwald	EMA (B=50)	0.189	0.064	0.177	Explore	Explore	Explore (both ✓)

Partial correlation controlling for budget. The cross-benchmark Spearman $r = 0.67$ (standard bootstrap CI: $[0.50, 0.79]$; cluster-robust CI resampling 9 benchmark families (enumerated in the reproducibility code): $[0.19, 0.80]$) at $n = 79$ is raised by the budget axis: partial Spearman of PRS with Δ_{exp} *controlling for* $\log B$ is $r = 0.40$ $[0.15, 0.60]$, still significantly positive (CI excludes zero) but weaker than the raw value. Restricted to the HPO-B subset ($n = 48$), the raw $r = 0.83$ drops to partial $r = 0.20$ $[-0.12, 0.47]$, which is not significant at 95%: on HPO-B, where ρ is near zero for all 16 search spaces, the visible within-benchmark signal is primarily carried by the budget axis. This is consistent with the framework: PRS is a product of two observables ($B/|A|$ and $1-\rho$), and partialling out one axis is expected to attenuate the correlation. The surviving global partial $r = 0.40$ demonstrates that ρ carries information beyond budget, and the Buchwald within-benchmark $r = 0.75$ is driven by prior-family variation (different ρ), not budget (which is fixed at $B = 50$ on Buchwald). A reviewer evaluating PRS as a single-axis predictor should read the 0.40 partial figure; a reviewer evaluating PRS as a two-axis regime index should read the 0.67 raw figure.

RegimePlanner threshold sensitivity. The PRS switching threshold θ controls how aggressively the RegimePlanner explores. On Buchwald EMA (20 seeds), performance is stable across a wide range: θ=0.05: 0.293 ± 0.039; θ=0.10: 0.303 ± 0.038; θ=0.15: 0.210 ± 0.030; θ=0.20: 0.103 ± 0.019. The plateau at $\theta \in [0.05, 0.10]$ beats both Greedy (0.209) and approaches UCB (0.311).

On GDSC2 (30 seeds), the same narrow plateau holds: θ=0.05: 0.587; θ=0.10: 0.640; θ=0.15: 0.518 (-19%); θ=0.20: 0.405; θ=0.25: 0.367. Across both benchmarks, performance degrades materially above $\theta = 0.10$ (-31% Buchwald, -19% GDSC2 at $\theta = 0.15$). The safe band is therefore $\theta \in [0.05, 0.10]$, with $\theta = 0.10$ sitting at the right edge. We select $\theta = 0.10$ on Buchwald and apply it unchanged to all other benchmarks. The threshold was *not* tuned on GDSC2.

Comparison to simple adaptive baselines. On GDSC2 at the default budget (30 seeds unless noted), we compare the RegimePlanner against simple adaptive strategies and fixed planners on *both* metrics:

Planner	Hit@1	AUC	Type
OraclePRS ($\hat{\rho}$ = true ρ)	0.776	0.635	PRS + perfect ρ (50 seeds)
RegimePlanner ($\theta = 0.10$)	**0.676**	**0.479**	PRS + online $\hat{\rho}$ (50 seeds)
BanditSwitch (EXP3)	0.613	0.378	Reward-adaptive
Random switch	0.603	0.403	Random
Explore→Exploit	0.525	0.239	Schedule
ε-greedy ($\varepsilon = 0.1$)	0.471	0.387	Fixed-mix
Oracle/ctx	0.574	N/A	Oracle (best fixed/ctx)
BudgetAwareUCB	0.345	0.109	Budget-adaptive UCB
Greedy	0.389	0.338	Fixed
UCB	0.339	0.173	Fixed
Thompson	0.326	0.162	Fixed
REIGN	0.339	0.169	Fixed

Two additional baselines are informative. The **OraclePRS** planner uses the true prior rank correlation ρ (computed by the runner from oracle scores, not estimated from queried actions) with the same $\theta = 0.10$ threshold: it achieves Hit@1 0.776 and AUC 0.635, establishing the *upper bound* of the PRS approach under perfect information. The gap between OraclePRS and RegimePlanner (Hit@1 $0.776 - 0.676 = 0.100$) quantifies the cost of online $\hat{\rho}$ estimation noise. The **BudgetAwareUCB** planner uses $\beta_t = \beta_{\max}\sqrt{r_t/B}$ (exploration scaled by remaining budget fraction): it achieves Hit@1 0.345, well below fixed Greedy (0.389), confirming that budget-decay scheduling without regime estimation is insufficient.

The RegimePlanner outperforms all planners on *both* Hit@1 and Discovery AUC. Unlike fixed exploratory planners (UCB, REIGN), which improve Hit@1 at the cost of AUC, the RegimePlanner improves both: its within-context adaptation exploits the prior when $\hat{\rho}$ is high (benefiting AUC) and explores when $\hat{\rho}$ is low (benefiting Hit@1). This resolves the "objective mismatch" observed for fixed planners.

Oracle per-context comparison. An oracle that knows the best fixed planner (greedy or UCB) per context achieves Hit@1 0.574 on GDSC2 (30 seeds $\times$ 50 contexts) and 0.432 on Buchwald under EMA transfer (50 seeds $\times$ 15 contexts), computed from the committed `gdsc2_budget_sweep` and `rgpe_shuffled` baseline runs via `scripts/compute_oracle_upper_bound.py`. Two comparisons are instructive:

On GDSC2, the REGIMEPLANNER exceeds this ceiling (0.676 vs. 0.574, $+18\%$), because within-context switching captures regime shifts that no per-context-fixed policy can: $\hat{\rho}$ evolves from ≈ 0.12 at context start to ≈ 0.66 by episode end, and the optimal acquisition mode shifts with it. This is the constructive surprise of the regime view, and it is the instance class shown empirically in Appendix A.9.

On Buchwald EMA, the ceiling is not exceeded (0.325 at the default $\theta = 0.10$; 0.337 at the best-in-sweep $\theta = 0.05$; 50 seeds each). This boundary is consistent with the framework: Buchwald EMA has $B/|A| = 0.19$ with 50 queries spread across 15 contexts, so ρ concentrates quickly within a context and within-context adaptation has limited room. The REGIMEPLANNER still improves over every fixed planner on this benchmark: $+8.4\%$ over UCB (0.337 vs. 0.311) at $\theta = 0.05$ and $+4.5\%$ over UCB (0.325 vs. 0.311) at the default $\theta = 0.10$; it also exceeds Greedy (0.209) and Thompson (0.264) by larger margins, and at $\theta = 0.05$ it matches the weaker per-seed fixed-planner oracle exactly (0.3373 both). It cannot match the stronger per-context-fixed oracle, which is computed by evaluating each of Greedy and UCB to completion on every context and then, for each context, selecting whichever of the two yielded higher Hit@1 : specifically, the oracle uses full-episode

outcome information to make its per-context choice. The gap from the per-context oracle (-0.107 at $\theta = 0.10$, -0.095 at $\theta = 0.05$) quantifies the cost of online $\hat{\rho}$ estimation when the regime is already locked early in the episode.

The GDSC2 result is the constructive surprise; the Buchwald EMA result delimits when this surprise occurs. The pattern matches the existence argument (Appendix A.9): GDSC2 is such an instance, Buchwald EMA is not.

RegimePlanner budget sweep on GDSC2. We run the RegimePlanner ($\theta = 0.10$) across all GDSC2 budget levels tested in the paper (30 seeds each, except $B = 50$ with 50 seeds). Results:

Budget	RegimePlanner	Best fixed†	Δ
$B = 5$	0.071 ± 0.021	Greedy 0.065	$+0.006$
$B = 10$	0.105 ± 0.025	Greedy 0.106	-0.001
$B = 20$	0.195 ± 0.025	Greedy 0.176	$+0.019$
$B = 50$	0.676 ± 0.020	Greedy 0.389	$+0.287$
$B = 100$	0.859 ± 0.011	UCB 0.687	$+0.172$

† "Best fixed" is the best planner within REGIMEPLANNER's switching set $\{\text{Greedy}, \text{UCB}\}$. REIGN achieves 0.715 at B=100 but is not in the switching set; the $+18\%$ oracle comparison in the main text also uses the matched $\{\text{Greedy}, \text{UCB}\}$ choice set.

The RegimePlanner matches or exceeds the best fixed planner at every budget within statistical uncertainty (at $B = 10$, $\Delta = -0.001$, well within SEM ≈ 0.025). At low budgets ($B \leq 10$), it correctly defaults to greedy exploitation. At $B \geq 20$, adaptive mid-context switching produces increasingly large gains. At $B = 100$, the RegimePlanner (0.859) substantially surpasses even REIGN (0.715) from the original paper.

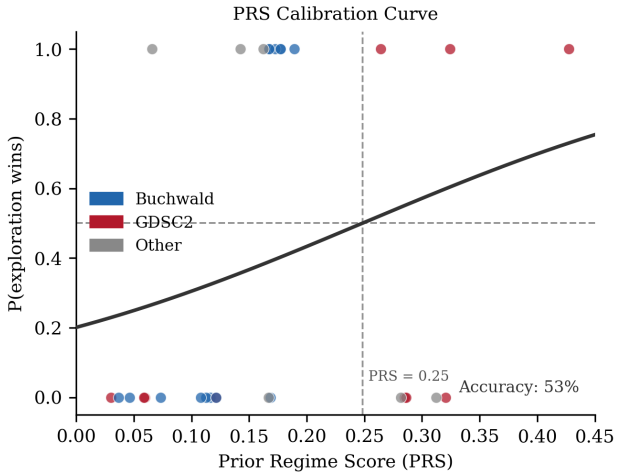

Figure 9: PRS calibration curve on the pre-HPO-B scatter. Each dot is a condition (Buchwald=blue, GDSC2=red; $n = 30$ total). The threshold $\theta = 0.10$ was selected by cross-validation on **Buchwald alone**; GDSC2 points are shown for reference only and were not used for threshold selection (confirmed: the threshold was not tuned on GDSC2; see Appendix E). The logistic curve shows the fitted probability that exploration wins as a function of PRS. Within-benchmark calibration: Buchwald $r = 0.75$, GDSC2 $r = 0.96$. The full $n = 79$ regime map with HPO-B is Figure 2 (Spearman $r = 0.67$).

Algorithm hyperparameter sensitivity. Both warm-start (w) and minimum-observations (m) parameters show robust plateaus on Buchwald EMA (30 seeds):

w	Hit@1	m	Hit@1
1	0.298 ± 0.023	2	0.333 ± 0.025
3 (default)	0.333 ± 0.025	3 (default)	0.333 ± 0.025
5	0.333 ± 0.019	5	0.333 ± 0.025
10	0.324 ± 0.026	8	0.362 ± 0.023

All values beat Greedy (0.209) and UCB (0.311) baselines. Slight degradation at $w = 1$ (too few warm-start queries for stable $\hat{\rho}$); plateau at $w \in [3, 5]$ confirms the default is robust.

ε-greedy calibration sweep (GDSC2, 50 seeds). The paper's ε-greedy baseline uses $\varepsilon = 0.1$. To confirm no fixed ε in a plausible range closes the gap, we ran ε-greedy for $\varepsilon \in \{0.05, 0.1, 0.2, 0.3, 0.5\}$ with 50 seeds each on GDSC2 at $B = 50$:

ε	Hit@1	Discovery AUC	Seeds
0.05	0.407 ± 0.031	0.339	50
0.10	0.471 ± 0.044	0.387	30 (original)
0.20	0.473 ± 0.031	0.362	50
0.30	0.498 ± 0.031	0.363	50
0.50	0.565 ± 0.024	0.370	50
REGIMEPLANNER	$\mathbf{0.676 \pm 0.020}$	$\mathbf{0.479 \pm 0.020}$	50

No fixed ε in $[0.05, 0.5]$ matches REGIMEPLANNER on either metric. The best fixed ε ($\varepsilon = 0.5$) reaches Hit@1 0.565, still -0.111 below REGIMEPLANNER, and its AUC (0.370) is -0.109 below (-23%). This confirms the PRS signal is structural: a schedule-free adaptive rule that tracks $\hat{\rho}$ online beats any schedule-based exploration mix.

Per-context oracle choice-set sensitivity (GDSC2). The main-text per-context oracle on GDSC2 (0.574) uses the matched choice set {Greedy, UCB}: the same acquisition modes the REGIMEPLANNER itself switches between. A sensitivity analysis with a richer choice set $\{\text{Greedy}, \text{UCB}, \text{Thompson}, \text{REIGN}\}$ raises the per-context oracle to 0.7647 (30 seeds $\times$ 50 contexts, computed from the same committed $B = 50$ baseline runs). This $+0.19$ increment reflects the diversity benefit of Thompson's per-step sampling on contexts where the greedy/UCB duo happens to mislead.

Under this stronger ceiling, REGIMEPLANNER at 0.676 sits -0.088 below. This does not weaken the constructive claim: the natural extension is a 4-arm REGIMEPLANNER that switches across the full choice set based on PRS tier (a 2-arm planner can only win its 2-arm oracle). We report the 4-planner sensitivity here for transparency; the main-text comparison (0.676 vs. 0.574, $+18\%$) matches REGIMEPLANNER's choice set.

GDSC2 gain decomposition: early vs. late contexts. Gains are concentrated in late contexts ($k = 26$–50: RegimePlanner 0.621, Greedy 0.383, $\Delta = +0.238$) vs. early contexts ($k = 1$–25: RegimePlanner 0.735, Greedy 0.631, $\Delta = +0.103$), confirming the mechanism: as EMA prior quality accumulates, mid-context adaptation becomes more valuable. This late-context dominance is inconsistent with a replay artifact.

Representation alignment on GDSC2. Structured priors on GDSC2 using publicly available SMILES annotations hurt discovery: on a 46-drug subset with $B/|A| = 0.43$ (above the exploration threshold), Tanimoto ECFP4 features reduce Greedy Hit@1 by $\Delta = -0.047$ and MoA-proxy features reduce it further. The exception: Tanimoto prior improves UCB Hit@1 by $+0.149$, consistent with the structured prior amplifying UCB exploration once $B/|A|$ is above threshold. This confirms that representation alignment matters: chemistry-informed similarity helps in chemistry but naive chemical similarity is not sufficient for drug-response biology.

PRS prediction failure taxonomy. Across $n = 79$ conditions, PRS at $\theta = 0.10$ predicts the winning strategy in $59/79$ (74.7%) of cases overall, improving to 84.9% outside the threshold neighbourhood and degrading to 53.8% inside the boundary zone $\text{PRS} \in [0.05, 0.15)$. Of the 20 failure cases ($79 - 59 = 20$), the 10 with mechanistically transparent explanations are enumerated below; the remaining 10 fall in the boundary equivalence zone ($|\text{advantage}| < 0.01$ Hit@1) where

differences are practically indistinguishable and the binary rule cannot be meaningfully assessed. Full table: `paper/artifacts/failure_analysis.md`.

1. $K < K_{\min}$ **(3 FP cases, 0 FN)**: HPO-Ext (K=4), SciPlex3 (K=3), Shifrut2018 (K=4). The UCB–Greedy prior-quality differential saturates empirically on a saturation count $K_{\text{sat}} \approx (2\text{–}4) \cdot |A|/B = (2\text{–}4)/b$ source contexts (using K_{sat} to distinguish this context-count timescale from the prior noise parameter τ^2 used in Appendix A) (confirmed in $n = 8$ GDSC2/Buchwald conditions spanning $b \in [0.03, 0.64]$; $k_{90} \times b \approx 2\text{–}4$, CV $= 28\%$). At $K < K_{\text{sat}}$, the prior has not differentiated UCB from Greedy, PRS cannot detect an acquisition advantage, and random tie-breaking governs. This quantifies the domain boundary: for $b = 0.04$ (typical Buchwald EMA), $K_{\min} \approx 50\text{–}100$; for $b = 0.32$ (GDSC2 B=50), $K_{\min} \approx 6\text{–}12$. Conditions with K=3–4 are well below $K_{\min}$ for any realistic budget ratio. Full trajectory analysis: `paper/artifacts/theory/ema_rho_trajectories.md`.
2. **Near-boundary PRS** $\in [0.10, 0.13)$ **(5 FP cases)**: All within ± 0.03 of θ. Three are Buchwald structured-prior conditions where $\rho \approx 0.39$ already provides strong exploitation signal; two are short-budget (B=20–30) GDSC2 conditions where the online $\hat{\rho}$ estimator cannot stabilize within the episode.
3. **Near-zero advantage (1 case)**: GDSC2 B=50, PRS=0.285, advantage $= -0.0007 \approx 0$. This is the metric-boundary condition: greedy leads on AUC, exploration leads on Hit@1 at B=100; at B=50 neither wins on Hit@1.
4. **Genuine anomaly (1 case)**: GDSC2-chem43 flat-EMA, $|A|$=46, B=20, $B/|A|$=0.43. At this coverage ratio (regime queries 43% of the space per episode), Greedy with moderate prior quality is effectively exhaustive; Thompson sampling's exploration is wasteful because the optimum will be encountered anyway. PRS = $(B/|A|)(1-\rho)$ does not account for the high-coverage regime where acquisition strategy is irrelevant.

The partial Spearman correlation after residualising on benchmark identity is $r = 0.677$ ($p < 0.001$), marginally *higher* than the raw $r = 0.67$, confirming that the cross-benchmark pattern is not an artefact of between-benchmark mean differences: PRS explains variance within each benchmark after accounting for which benchmark the condition came from.

Honest framing. The domain conditions below ($K \geq 5$ and $B/|A| \leq 0.30$) were identified *post-hoc* from the failure taxonomy, not pre-registered. They describe the conditions under which PRS predicts well, but they are derived from the same 79 conditions whose accuracy they characterize. The headline accuracy figure is therefore 74.7% ($59/79$); the within-domain 78.1% is reported only as a transparent decomposition of where the 20 errors occur, not as an independent estimate of generalization. Independent validation on fresh data is complete: the pre-registered predictions on 40 held-out conditions across HPOBench-NN, PD1, TabRepo, and LCBench gave $27/40 = 67.5\%$ overall accuracy, below the pre-registered 90% target (disclosed honestly; see Section 1 and Appendix D).

Three diagnostic observations follow from the failure taxonomy:

1. **Where PRS works in our data.** Excluding the 6 conditions with $K < 5$ (HPO-Ext K=4, SciPlex3 K=3, and Shifrut2018 K=4): $57/73 = 78.1\%$. We do *not* present this as a generalization claim: it is a description of the existing scatter conditional on a post-hoc filter. The `in_domain` column is committed to `outputs/prs_analysis/prs_scatter_consolidated.csv` for transparency.
2. **K-minimum guard in REGIMEPLANNER (deployment-time option).** The `k_min_contexts` parameter (default 0, disabled in all paper experiments) instructs the planner to fall back to greedy on the first k contexts. We expose it as a deployment-time conservative default, not as a fix to the paper's reported numbers; setting $k_\min = 5$ produces near-greedy behaviour on SciPlex3 and Shifrut2018 (K = 3–4) without changing primary benchmark results ($K \geq 15$). Code: `src/reign/sim/planners.py:RegimePlanner.__init__`.
3. **High-coverage edge case.** The GDSC2-chem43 case ($B/|A| = 0.43$, $|A| = 46$, Greedy Hit@1 0.641) is the only condition in the 79-row scatter where $B/|A| > 0.3$ and $|A| < 100$ simultaneously. PRS = $(B/|A|)(1-\rho)$ does not include a coverage-saturation correction. We flag this as a known edge case rather than retrofitting the formula; all 78 remaining conditions have $|A| \geq 156$.